IEEE Access
Multidisciplinary | Rapid Review | Open Access Journal

Received October 18, 2021, accepted November 16, 2021, date of publication November 19, 2021,
date of current version December 9, 2021.

Digital Object Identifier 10.1109/ACCESS.2021.3129608

Fractional-Fuzzy PID Control Approach of Photovoltaic-Wire Feeder System (PV-WFS): Simulation and HIL-Based Experimental Investigation

BADREDDINE BABES[1], FAHAD ALBALAWI[2], NOUREDDINE HAMOUDA[1], SAMI KAHLA[1], AND SHERIF S. M. GHONEIM[2], (Senior Member, IEEE)

[1]Research Center in Industrial Technologies (CRTI), Cheraga, Algiers 16014, Algeria
[2]Electrical Engineering Department, College of Engineering, Taif University, Taif 21944, Saudi Arabia

Corresponding authors: Badreddine Babes (elect_babes@yahoo.fr) and Sherif S. M. Ghoneim (s.ghoneim@tu.edu.sa)

This work was supported by the Taif University Researchers Supporting Project through Taif University, Taif, Saudi Arabia, under Grant TURSP-2020/97.

ABSTRACT The utilization of solar photovoltaic (PV) generator as a power source for wire feeder systems (WFSs) of arc welding machines is one of the promising domains in solar PV applications. This article proposes a new type of welding WFS and investigates the PV penetrated energy systems. The proposed system comprises of a solar PV generator, a DC/DC buck converter, and a permanent magnet DC (PMDC) motor. The power of the proposed standalone solar photovoltaic-wire feeder system (PV-WFS) can be widely improved using an intelligent fractional-order fuzzy proportional integral derivative (FO-Fuzzy-PID) regulator based on perturbing and observe (P&O) MPPT method. In this article, a FO-Fuzzy-PID regulator is also designed for a PMDC motor driven welding WFS system. Which will then control the wire feed rate of the welding WFS system. Furthermore, the dynamic reaction of the proposed solar PV-WFS depends on the coefficients of these FO-Fuzzy-PID regulators, which are adjusted by a meta-heuristic tuning algorithm based on particle swarm optimization (PSO) technique. The proposed strategy is tested using MATLAB simulations and experimentally verified in real-time on a Hardware-in-the-loop (HIL) testing platform using a dSPACE 1104 board-based laboratory setup. Simulation and experimental results are acceptable and demonstrate the effectiveness, precision, stability, and dynamic reaction of the suggested optimized wire feeder regulating system and the considered intelligent P&O MPPT technique.

INDEX TERMS Buck converter, fractional-order fuzzy PID regulator, MPPT technique, PSO algorithm, PV module, wire feeder system (WFS).

LIST OF ABBREVIATIONS

FLC	Fuzzy Logic Control
GMAW	Gas Metal Arc Welding
GTAW	Gas Tungsten Arc Welding
HE	Hourly Efficiency
HIL	Hardware-In-the-Loop
IHPS	Isolated Hybrid Power System
ITAE	Integral of Time Multiply Absolute Error
I&C	Incremental and Conductance
LTI	Linear-Time-Invariant
MPPT	Maximum Power Point Tracking
MOA	Metaheuristic Optimization Algorithm
NN	Neural Network
PV	Photovoltaic
P&O	Perturb and Observe
PMDC	Permanent Magnet DC Motor
PSO	Particle Swarm Optimization Algorithm
PID	Proportional Integral Derivative
PV-WFS	Photovoltaic-Wire Feeder System
RCD	Real Climatic Data
SMAW	Shield Metal Arc Welding
SMC	Sliding Mode Controller
STC	Standard Test Condition
TSC	Top Shading Condition

The associate editor coordinating the review of this manuscript and approving it for publication was Bidyadhar Subudhi.

WFS	Wire Feeder System
ZCES	Zero-Carbon Energy Source

I. INTRODUCTION

The disappearance of traditional energy sources has shifted the focus of the world's attention to unconventional energy sources like wind energy and solar PV systems. Solar-based PV power generations are of major importance because of low maintenance and no mechanical device included in the energy conversion process. According to the report, Algeria is one of the sunniest countries in the world [1]. It receives an average of 10 hours of sunlight per day, which is equivalent to 8 kWh/m^2, and approximately equal to one liter of gasoline [1]. These advantages make the production of electricity from solar energy exciting and vital for Algerian localities, especially for isolated places such as the desert or rural regions, in which the complexity of fuel transportation and the absence of a power grid render the utilization of traditional resources impractical. Welding in such environments is challenging because it necessitates a reliable power source to feed the electrical components of the arc welder. The welding wire feeder system (WFS) of an arc welder runs on electrical energy produced by solar PV generators. The quantity of metals dropped in welding workpiece is fed to a arc welder in a regulated manner using a standalone PV-WFS. The PV generators transfer solar energy into electricity to operate PMDC motor-based welding WFS. The success of a standalone solar PV-WFSs depend on the ability of the MPPT controller to properly function the PV generator even under changeable weather conditions. The goal is to gain maximum energy from the PV generator under any weather condition. Hence, the reliability of the MPPT regulator is of great importance to the efficient operation of PV-WFS. The MPPT control is a defy because the PV generator's sunshine energy input flux may vary at any instance. Indeed, the PV generator is considered a nonlinear complex system. Because of these factors, designing a suitable MPPT regulator setup is challenging to build. On the other hand, the performance required in choosing the wire feeder regulator is critical, since the arc welder must be able to feed the welding wire at a high rate during a few milliseconds in conjunction with the PMDC motor in the welding WFS. The latter demands the achievement of high dynamic behavior in order to track the required welding wire speed. Fluctuations in torque demand are large since a 400 A rated arc welder is required to form welding joints with electrodes varying in diameter between (0.6 mm -1.6 mm). The material formation of a welding wire (or consumable electrode) can also change greatly [2]. Therefore, for perfect wire feed speed tracking, the PMDC motor of the welding WFSs necessitates a consistent wire feed speed regulator.

A. MOTIVATION

This document suggests a new type of WFS system. It discusses the PV integrated energy systems to form a standalone solar PV-WFS and recommends implementing a FO-Fuzzy-PID regulator to maximize power through a PV generator and enhance welding quality. Solar energy is the best way to generate sustainable energy [3]. The amount of energy generated by a PV generator changes depending on the weather. Therefore, the maximum energy is often obtained from a PV generator under various temperature and radiation by resorting to MPPT methods [4]. Achieving MPP, a variety of methods like P&O, incremental and conductance (I&C), fuzzy logic (FL), neural network (NN), and sliding mode control are proposed in the literature [4]–[8]. Nevertheless, the commonly used approaches comprise P&O and I&C methods. Due to the lower fluctuations in variable step-size P&O during MPP determination It is the perfect choice here, as well as being more commercially viable.

One of the crucial considerations for MPPT programmers is to choose a suitable control algorithm along with the MPPT control. In general, the MPPT control is performed using either one of the two approaches [9]. The first is the direct method, often known in the literature as the duty ratio-based MPPT control. In this situation, the MPPT algorithm determines the duty ratio and sends it to the DC/DC converter immediately. There is no extra process; another control loop between the MPPT controller and the DC/DC converter. To put it another way, it is the MPPT algorithm that determines the appropriate duty ratio at which the PV system reaches MPP. The second option is the indirect method, often called voltage or current-based MPPT control. Here, the MPPT merely creates a reference voltage or current, in this case a voltage/current regulator is used to regulate the duty cycle of the converter such that the photovoltaic voltage/current follows the former reference voltage or current. Structurally, the direct approach is much simpler than its counterpart because the MPPT adjusts the duty ratio without an additional control loop. However, because the direct approach depends on the characteristic of power against duty ratio, the value of the duty ratio may change drastically when the radiation changes. In addition, when the load fluctuates, the direct approach displays significant transient variations [10]. This condition is critical for a standalone solar PV generator, where the DC/DC converter linked to an isolated load. It causes the PV voltage/current to diverge from MPP [11]. In another manner, the indirect approach is described by the power against voltage or current curves. It is less influenced by the fast changes in irradiance since the voltage/current is limited within a much narrower range other than the duty ratio [12]. Thus, an alteration in irradiance level leads to a lesser change in voltage/current. In addition, since the power against voltage/current curve depends only on irradiance and temperature, the voltage/current is unaffected by the topology of the DC/DC converter. So, even if the load changes, the voltage/current remains nearly constant because the voltage/current regulator pushes the operating point to be close to MPP. It allows for more accurate tracking as the load varies. The above discussion shows that indirect control

provides an efficient solution to increase the reliability of a standalone solar photovoltaic-wire feeder system (PV-WFS).

This indirect method involves MPPT voltage-based regulator in series with a voltage regulator or an MPPT current-based regulator in a series with a current regulator. Since the PV voltage remains nearly constant at MPP under radiation variations, voltage-oriented MPPT is regarded a quick MPP tracking method [13]. Nevertheless, the effectiveness of this approach depends on the design of the voltage controller. The voltage-oriented MPPT has been assembled with a PI regulator, which is employed in the voltage control loop in Bianconi *et al*. [14], and sliding mode regulator (SMC) in Maissa *et al.* [15]. However, the former has big voltage oscillations that must be reduced, while the second has a variable switching frequency [16]. On the other hand, the benefits of current-oriented MPPT include reduction in voltage oscillations of the output PV generator, increase in MPP tracking accuracy, and reduction in the system's overall complexity. It enhances, as a result, the use of the PV generator, making it a better option than voltage-oriented MPPT control [14].

According to several studies on the indirect control method, the performance and robustness ensured in a closed-loop generally depend on the regulators' structure and the optimization method utilized to optimize the regulator coefficients. The PID regulators are mostly exploited in current-oriented MPPT. This is because of its ease of use, stability and flexibility in adjusting its coefficients [17]. The utilization of FO derivatives and integrals can improve the performance of PID regulators [18].

During the last few decades, FO regulators have gained great importance in the scientific field due to their additional flexibility and good structure [19], [20]. FO-PID regulators have two other coefficients (α and β) in addition to the three well-known gains of traditional PID regulators; proportional (K_P), integral (K_I) and derivative (K_D) gains. The (α) and (β) are the power of (s) in integral and derivative operations. It improves the stability and flexibility of FO-PID regulators; as a result, it has better dynamic performance than standard PID regulators [21]. The quality of the FO-PID regulator is greatly influenced by the correct set of values for (K_P, K_I, K_D, α, and β) chosen to meet the required performance of a user for a certain process plant. It has been documented in various studies that the proper adjusting of the FO-PID regulator coefficients improves its performance and confers robustness to the system. According to an expert knowledge database, a FLC uses fewer calculations to make decisions, but it has a limited ability for new rules [22]. Therefore, this problem can be solved by integrating FLC with FO-PID regulators.

The role of the FLC is to update the FO-PID regulator based on error and change of error. In comparison to a conventional FO-PID regulator, it might be an excellent alternative [22]. Optimization techniques have an immense influence in enhancing the competency of the FO-Fuzzy-PID regulator by establishing its relevant parameters. The proposed work investigates the applicability of PSO-based FO-Fuzzy-PID regulator to current-oriented MPPT and speed regulation of PV-WFS. The PSO algorithm is a meta-heuristic technique of swarm intelligence approach that simulates the psychosocial behavior of collective organisms (Birds in flight, shoals, etc). It is being used to solve nonlinear and continuous problems and adapt single-objective and multi-objective problems [23], [24]. Consequently, it is a suitable optimization approach for regulator design. These benefits prompted us to use the PSO method to improve the FO-Fuzzy-PID regulator's decision variables.

Thus, in this study the suggested PSO-based FO-Fuzzy-PID regulator performs well at different operating points. The capacity of the current regulator is verified by analyzing and comparing the outcomes with PSO-based PID, FO-PID, and FLC regulator. Literature survey reveals that the wire feed speed control of a welding WFS mainly relies on the structure of the regulators, and the optimization process used to find the optimum regulator coefficients [25]. PID regulators are today in service in most industrial control loops, because of their simplicity and reliability. Wire feed speed of welding WFS system may be controlled with a conventional PID regulator as reported by Chaouch *et al*. [26]. However, there is no precise mathematical method for determining the suitable PID factors (such as K_P, K_I and K_D).

Typically, these factors are often calculated using empirical methods and, as a result, may not be effective, which is one of the major drawbacks of this kind of regulator. The optimization-based methods provide a general framework for finding optimal PID regulator parameters; nevertheless, the PID regulator still has low robustness compared to the nonlinear regulator when the system encounters multiple challenges from the operating conditions. Therefore, more advanced control strategies should be applied to deal with the speed control difficulties in welding WFS systems. With high robustness and satisfactory control performance in nonlinear systems, FO-Fuzzy-PID regulators are increasingly drawing the attention of researchers. This encouraged us to investigate the potential of using the PSO algorithm to improve the wire feed speed regulation of the FO-Fuzzy-PID speed regulator in the welding WFS system. Thus, this study also presents PSO-based FO-Fuzzy-PID speed regulators to be employed rather than the PSO-based PID, FOPID, and FLC speed regulators. Therefore, the PSO algorithm is used to adjust regulator coefficients (K_P, K_I, K_D and K_U) as input and (α, β) as output scaling coefficients; α and β are used as fractional order differ-integrals.

In addition, to complete the wire feed speed regulation, the PMDC motor speed regulator is associated with the welding WFS system. To demonstrate the complete examination of the present control approach, simulation results under various situations were run in MATLAB/SIMULINK. The results demonstrate that the considered PSO-based FO-Fuzzy-PID regulator alleviates the PV power and motor speed variations and decreases the settling time significantly, as compared to the PSO-based PID, FOPID, and FLC control. This study is

expected to give valuable insight into the definitive selection of an acceptable control structure for a stand-alone solar PV-WFS plant.

B. RELATED WORK AVAILABLE IN THE LITERATURE

Researchers have used several FOPID regulators for MPPT and speed regulation studies because they offer more freedom and flexibility than conventional PI or PID regulators [27]–[29]. However, FOPID regulators are model-dependent and work well only when a precise mathematical model is offered. The problem mentioned above can be solved by using a FLC, in which the behavior of FLC-based systems might be improved by using FO calculus. From the literature, authors have proposed the FO-Fuzzy-PID regulators to improve the transient stability of many systems. Several decomposed combination structures of fractional-order hybrid fuzzy PID regulators with their relevant comparative advantages were investigated in Das *et al*. [30] for three kinds of oscillatory non-integer plants. On the other hand, a novel design structure for a FO-Fuzzy-PID regulator is presented in Das *et al*. [31] to handle two distinct processes, including a nonlinear plant and an open-loop unstable plant.

Pan and Das [32] have suggested a Fractional-order Hybrid Fuzzy regulator for load frequency control of renewable energy resources (RER) via chaotic PSO algorithm and claimed better results than traditional counterparts. In Jesus and Barbosa [33], a FO-Fuzzy-PD+I regulator is introduced, and excellent results are obtained when compared to a traditional Fuzzy-PID regulator. In Mahto and Mukherjee [34], a FO-Fuzzy-PID regulator is examined for frequency and power regulation of an isolated hybrid power system (IHPS) and superior results are obtained when compared with the PID and Fuzzy-PID regulator. As a consequence, the combination of FLC and FOPID regulators outperformed the traditional Fuzzy-PID regulators in terms of control.

A FO-Fuzzy-PI+I regulator has been investigated by Beddar *et al*. [35], where the PSO method was developed for choosing the optimum regulator coefficient value. Furthermore, several soft search techniques such as genetic algorithm (GA) [36], ant colony optimization (ACO) algorithm [37], PSO algorithm [35], cuckoo search algorithm (CSA) [38], artificial bee colony (ABC) algorithm [39], and IJAYA algorithm [40] have been introduced for optimally calculating the FO-Fuzzy-PID regulator parameters to enhance the system stability. The PSO method has recently emerged as one of the most important and widely used optimization algorithms for solving various problems in a variety of disciplines [41]. Flexibility and simplicity for process optimization are among the key features of PSO [42], [43]. PSO is based on a swarm intelligence model that is inspired by the collective behavior of animals such as fish and birds. This degree of intelligence is unattainable for individual swarm member, but it may be achieved via collaboration. According to the above literature review, the FOPID regulators were proposed by hybridizing with FLCs; therefore, its application with the PSO algorithm will open up a new study topic for scientific communities in the framework of PV-WFS. This characteristic prompted the authors to consider the PSO-based FO-Fuzzy-PID regulators for the PV-WFS to overcome the control problems of large power ripples, settling time, and high overshoot.

C. INNOVATIONS AND CONTRIBUTIONS

This paper is a continuation of the previous work [25], and aims to facilitate HIL testing of solar PV-WFS systems with a focus on the implementation of the FO-Fuzzy-PID regulator. According to the above analysis, this work can contribute to the subsequent points:

1. Suggest a new optimal robust FO-Fuzzy-PID controller that combines fuzzy logic with fractional PID controller to enhance wire-feed speed regulation in welding WFSs while accounting for solar power penetration;
2. The suggested FO-Fuzzy-PID controller (i.e., fuzzy logic, PID controller) is optimally determined based on a PSO algorithm, to reduce the integral time-weighted absolute error (ITAE) cost function of the solar PV-WFS. Where the PSO algorithm has been utilized to achieve the desired target. It is the first time to apply this algorithm to select optimal parameters for MPPT and wire fedd speed problems;
3. The effectiveness of the suggested robust FO-Fuzzy-PID controller is tested and verified through HIL testing platform using a dSPACE DS1104 controller board;
4. Comparing with other controllers that were utilized in MPPT control and wire feed speed studies for improving the solar PV-WFS performance (e.g. traditional PID controller, FLC and FOPID controller).

D. ARTICLE ORGANIZATION

Here is a breakdown of the article's structure: the second part will describe and model the considered PV-WFS. In the third part, an introduction to fractional calculus and PSO method will be introduced for utilization with FO-Fuzzy-PID regulators of PV-WFS, whereas in the fourth and fifth parts, all the suggested FO-Fuzzy-PID regulators will be explained. The sixth part will provide and discuss the simulation and experimental tests of all the suggested FO-Fuzzy-PID regulators. Finally, the seventh part concludes the findings of the work.

II. DESCRIPTION AND MODELING OF THE PV-WFS

The studied PV-WFS, represented in Fig. 1, comprises four major components: a PV generator, DC/DC buck converter, and a battery bank coupled to the WFS driven by a PMDC motor. A DC/DC buck converter is employed to regulate the PV generator current. The control system adopts the indirect MPPT control loop. In this system, the primary FO-Fuzzy-PID current loop regulates the PV current (I_{pv}) by adjusting the duty ratio (D_1), on the other hand, the MPPT controller keeps follow the MPP by changing the reference of the inductor current. An improved P&O method gives the reference current. Because it makes the analysis easier, a

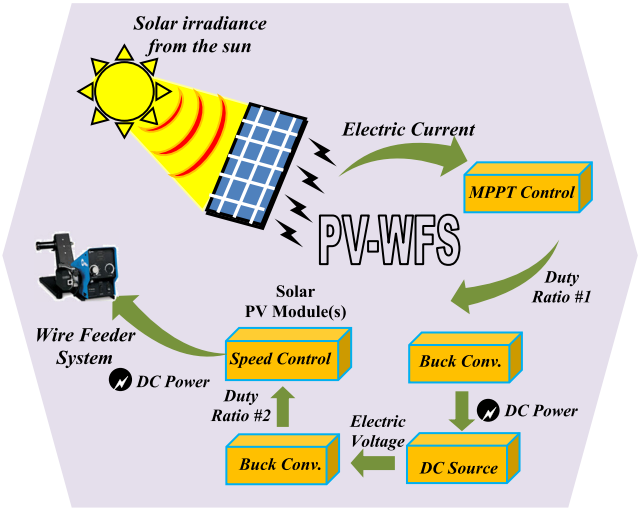

FIGURE 1. Description of the studied solar PV-WFS.

continuous DC power supply is used, allowing to represent the PV generators with a battery charge or PV generators with another stage of power conversion [44]. The second comprise a DC power supply coupled to the WFS through a second DC/DC buck converter. In WFS's velocity control loop, the velocity error is calculated by comparing the real PMDC motor velocity and the reference velocity is transmitted to the second FO-Fuzzy-PID controller. Fig. 1 illustrates the suggested PV-WFS system, which will be modeled later.

A. PV GENERATOR MODEL

PV generator mostly consist of PV cells and modules. It receives light photons and emits an electron charges, and can transform solar energy directly into electricity [45]. The amount of electricity produced by a PV generator is significantly influenced by environmental conditions [46]. The PV cell is a nonlinear system that can be modeled as a current source with dependent voltage source [47]. The most common PV cell models are single-diode and double-diode [47]. In this article, to characterize the features of PV cells, we employ the single-diode model. Fig. 2 depicts a simplified model of a single solar cell, which consists a diode (D), a shunt resistor (R_p), and a serial resistor (R_s). Utilizing kerchief's law, the output current of the solar PV cell is given by [48]:

$$I_{pv} = I_{ph} - I_d - I_{R_p} \tag{1}$$

$$I_{pv} = I_{ph} - I_o\left[\exp\left(A(V_{pv} + R_s.I_{pv}\right) - 1\right] - \frac{V_{pv} + R_s.I_{pv}}{R_p} \tag{2}$$

where, I_{ph} is the generated photo-current (A), I_{pv} represents the PV current (A), I_d is the diode current (A), V_{pv} denotes the PV voltage, I_0 is the reverse saturation current (A), A is the idealization coefficient for the diode (from1 to 2).

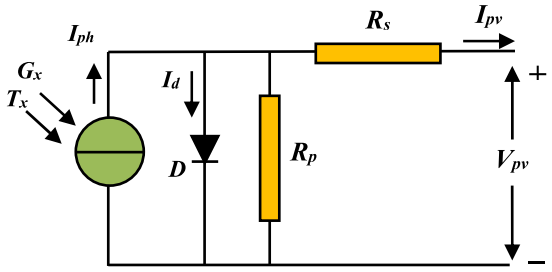

FIGURE 2. A simplified model of a single solar cell.

Other terms in Eqs. (1) and (2) can be obtained by

$$I_{ph} = I_{sc} + \left[K_i\left(T - T_{ref}\right)\right]\frac{G}{1000} \tag{3}$$

$$I_S = I_{rs}\left(\frac{T}{T_{ref}}\right)^3 \exp\left[\frac{q.E_{go}}{K_o.A}\left(\frac{1}{T_{ref}} - \frac{1}{T}\right)\right] \tag{4}$$

$$I_{rs} = \frac{I_{sc}}{\exp\left[\frac{q.V_{oc}}{N_c.K_o.A.T}\right] - 1} \tag{5}$$

where T_{ref} is the reference temperature of the cell, I_{rs} is the leakage current at T_{ref}, and I_{sc} is the short-circuit current, G is the solar radiation, E_{go} is the band-gap energy of the semiconductor ($E_{go} = 1.12$ ev) and K_i is the short-circuit temperature factor (0.0024 A/K). q is the electron's charge (1.6×10^{-19} C), K_o is the Boltzmann's coefficient ($1.38 \times 10{-}23$ J/K), V_{oc} is the open-circuit voltage and N_c is the number of cells. The energy of one cell is not enough to operate the PV-WFS system, thus, PV cells are connected together in shunt and in series to generate sufficient energy, for running a WFS at normal working conditions. The mathematical representation of PV system is expressed by Eq. (6)

$$I_{pv} = I_{phg} - I_{og}.\left[\exp\left(A_g\left(V_{pv} + R_{sg}.I_{pv}\right)\right) - 1\right] - \frac{V_{pv} + R_{sg}.I_{pv}}{R_{pg}} \tag{6}$$

where $I_{phg} = N_p \times I_{ph}$(A) and $I_{og} = N_p \times I_o$(A) are the leakage and the photo-current of the PV generator. I_{pv} represents the PV generator current, V_{pv} is denotes the PV generator voltage, R_{pg} and R_{sg} are the shunt and the series equivalent resistance related to the PV generator. $A_g = A/N_s$ is the PV generator coefficient, N_s and N_p are the number of cells connected in series and shunt. The PV generator model is depicted in Fig. 3.

The considered PV generator can be represented using Eqs. (1) to (6). A real PV module ND-240QCJ was proposed as a standard module [49] to develop the PV model. Table. 1 lists the main parameters of the PV generator under Standard Test Conditions (STC).

Fig. 4 shows the generated outputs in (I_{pv}-V_{pv}) and (P_{pv}-V_{pv}) characteristics of PV generator at $T = 25$ °C and various radiation conditions. To get the desired voltage from the PV generator, 120 cells must be linked in series. This system achieves the required voltage by applying a gain on the cell voltage equal to the total number of cells.

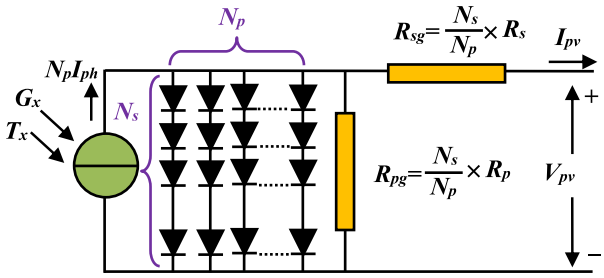

FIGURE 3. PV generator model.

TABLE 1. Specification for the PV generator.

Details	Value
Maximum power	240 W
Current at MPP	8.20 A
Voltage at MPP	29.31 V
Open-circuit voltage	37.52 V
Short- circuit current	8.75 A
Temperature constant of I_s	0.53m A/K
Temperature constant of V_{oc}	-36m V/K
Number of cells	60 cell

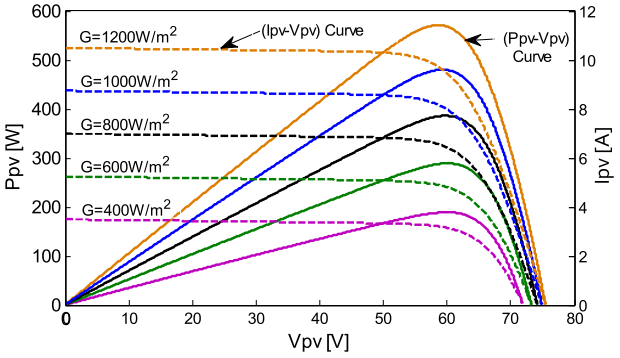

FIGURE 4. (I_{pv}–V_{pv}) and (P_{pv}–V_{pv}) characteristic curves of the PV generator at $T = 25$ °C and various radiation conditions.

B. DC/DC BUCK CONVERTER MODEL

The DC/DC buck converter delivers an output voltage equal to or lower than the source voltage. All equipment in the considered PV-WFS are connected to each other by two DC/DC buck converters. The primary converter is placed between the output voltage of the PV generator (V_{pv}) and the DC supply voltage (E) to force the PV generator to function at the MPP. The second converter is inserted between the DC supply voltage (E) and the PMDC motor to operate the welding WFS at the preferred wire feed velocity.

The DC/DC buck converter utilized for the PV generator is constituted of a PV modules, an inductor (L), an electronic switch (S), a diode (D), an output capacitor (C), as depicted in Fig. 5.

The DC/DC buck converter is controlled by the PWM modulator's signal input $u(t)$. Its operating principle can be determined by duty ratio (D) and switching period (T_s) using

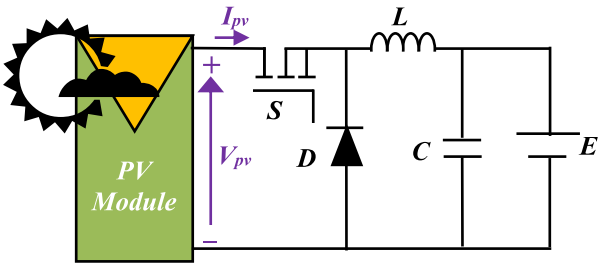

FIGURE 5. Schematic representation of the PV generator with a DC/DC buck converter.

TABLE 2. Specifications for the DC/DC buck converter.

Details	Value
Inductance	4 mH
Capacitance	0.50 µF
Working frequency	20 kHz

the following formula

$$u(t) = \begin{cases} 1, & 0 \le t < DT_s \\ 0, & DT_s \le t \le T_s \end{cases} \quad u(t - T_s) = u(t)\ \forall t \tag{7}$$

Using Kirchhoff's equations to the electrical system of Fig. 5, which has two distinct modes of action, "*on*" and "*off*", the switching model of converter may be found in a simple format using Eq. (8)

$$\dot{I}_{pv} = \frac{\dot{V}_{pv}}{L} D + \frac{1}{L}\left(V_{pv} - E\right)(1 - D) \tag{8}$$

This formula is named switched model because it describes the dynamic behaviors of the DC/DC converters [50], [51].

The optimum values of the inductor (L) and capacitor (C) for the DC/DC buck converter are carefully calculated by (9):

$$L_{\min} = \frac{D\,(1 - D)\,V_{pv}}{f_s \Delta I} \tag{9}$$

$$C_{\min} = \frac{D\,(1 - D)\,V_{pv}}{8 L f_s^2 \Delta V} \tag{10}$$

where ΔV and ΔI are the capacitor voltage and inductor current oscillations, and f_s is the working frequency of the converter. The component values for the considered converter are computed for a current oscillations of 5 %, a capacitor voltage oscillations of 10 %, a rating power of 480 W, a supply voltage up to 200 V, a capacitor voltage within 12 to 48 V, and a working frequency of 20 kHz. Table 2 summarizes the design specifications of the considered converter.

C. ASSEMBLY WFS AND GMAW PROCESS MODEL

Fig. 6 depicts the WFS of the GMAW process. The wire feeding servo motor is a feedback-controlled device that can deliver wire at a controlled V_f (m/s) speed from a wire bobbin to the welding process. In most of the time, V_f is maintained constant at V_f^*, which is the desired speed.

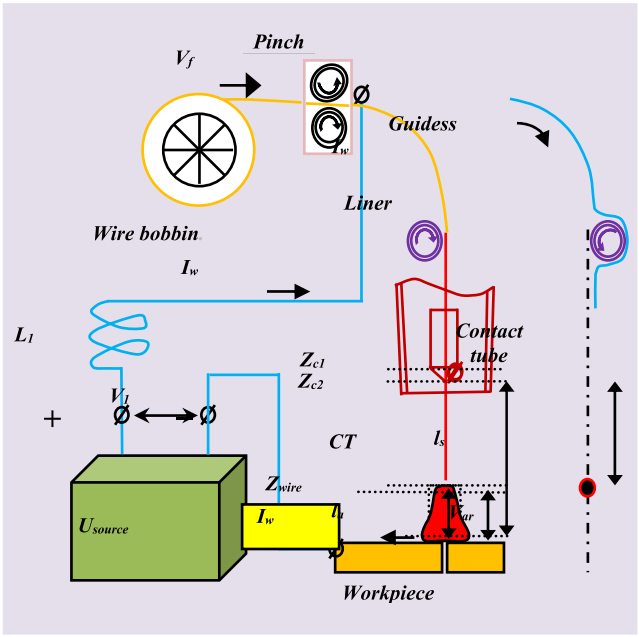

FIGURE 6. Physical illustration of the WFS used in GMAW process.

The electrical circuit of the GMAW process is mathematically modeled as follows:

$$V_1 = L_1 \frac{dI_w}{dt} + R_1 I_w + V_{arc} \tag{11}$$

where V_1 is the open-circuit voltage of the arc welder unit, I_w is the welding current, R_1 is the equivalent resistance of the arc welder unit plus the resistance of the conductors, and L_1 is the inductance of arc welder unit. The mathematical model of the arc voltage V_{arc}, can be written as follows:

$$V_{arc} = k_a l_{arc} + k_p I_w + V_c \tag{12}$$

where k_a, k_p, V_c are parameters of arc, and l_{arc} is the arc length. The mathematical representation of l_{arc}, is written as follows:

$$\frac{dl_{arc}}{dt} = V_m - V_f \tag{13}$$

where V_m indicates the wire fusion rate:

$$V_m = k_m I_w \tag{14}$$

where k_m represents the wire fusion rate constant. The mathematical equation of the power supply V_1, is written as follows:

$$V_1 = (R_u + k_1 I_w)\, k_0 \tag{15}$$

where R_u is the control signal of the power supply, k_0 is coefficient of power source and k_1 is feedback coefficient.

D. MODELING OF PMDC MOTOR WIRE-FEEDING SYSTEM (WFS)

WFSs comes in a variety of configurations. The PMDC motor is the most popular type because it provides high efficiency with negligible vibration [38]. A PMDC motor uses a DC/DC buck converter to transfer electrical power from a PV generator and a DC supply voltage into mechanical power by rotating a rotor via magnetic coupling.

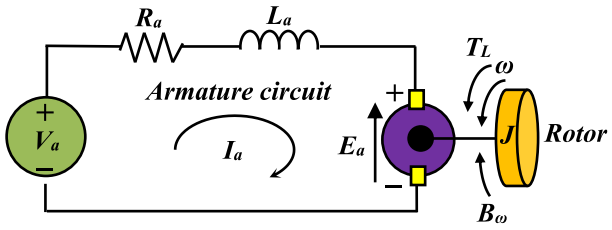

FIGURE 7. Circuit schematic of the wire-feed servo motor.

TABLE 3. Specifications for the PMDC motor of WFS.

Details	Value
Motor resistance (R_a)	1.25 Ω
Motor inductance (L_a)	0.95 mH
Motor inertia (J)	$1*10^{-7}$ kg.m^2
Friction factor (B)	$1.30*10^{-3}$ N.m.s/rad
Velocity constant (k_a)	0.05 V.s/rad
DC supply voltage (E)	24 V

The circuit schematic of the wire-feeding system is depicted in Fig. 7. The armature circuit of the PMDC motor can be represented by an inductance (L_a) in series with resistance (R_a) in cascade with a generated voltage (E_a), that opposes the DC input voltage (V_a).

Applying Kirchhoff's law to the armature circuit, the torque formula, the back EMF formula, and the movement formula, the dynamic behavior of a PMDC motor can be expressed as follows [52]:

$$V_a = R_a I_a + L_a \frac{dI_a}{dt} + k_a \omega \tag{16}$$

$$T_{em} = B\omega + J\frac{d\omega}{dt} + T_L \tag{17}$$

$$T_L = 3.27 + 0.38 \sin(2 * \pi * f_d * t) \tag{18}$$

where, I_a and V_a are the line current and voltage of the PMDC motor, R_a is the motor resistance, L_a is the motor inductance, J represents the moment of inertia, B denotes the friction factor, k_a represents the velocity constant. ω represents the mechanical speed. T_L and f_d are the external torque and turbulence frequencies.

Table 3 lists the specific components used to simulate the PMDC motor of the WFS.

III. GENERAL IDEA ABOUT FRACTIONAL CALCULUS, FO-FUZZY-PID REGULATOR, AND PSO METHOD

The proposed standalone PV-WFS needs a feedback regulator that directly adjusts the duty ratio of a DC/DC buck converter to ensure the optimal power in the presence of solar irradiance fluctuations and speed variations. For this reason, this section introduces the design methodology of a robust FO-Fuzzy-PID regulator that improves the response time of a standalone PV-WFS and increases its robustness against changes in wire feed speed and solar irradiance. The

FOPID regulator was chosen as the primary regulator due to its flexibility and ease of implementation. Nevertheless, in this article the FOPID regulator has been added to FLC system to enhance its time-domain performance and disturbance attenuation capacity. The PSO algorithm is used for the optimal selection of FO-Fuzzy-PID regulator gains. The resulting PSO-based FO-Fuzzy-PID regulator offers a considerable enhancement in the transitional and steady-state phases of the standalone PV-WFS. This part starts with a basic introduction in fractional calculus, following that, the improved FO-Fuzzy-PID regulator will be designed.

A. FRACTIONAL CALCULUS

Fractional calculus takes a prominent place among the basic branches of mathematics. In FO calculus, d^{α}/dt^{α} can have fractional negative or positive α values. The following equation is a simplified form of the operator FO [53]:

$$ {}_aD_t^{\alpha} = \begin{cases} \dfrac{d^{\alpha}}{dt^{\alpha}}, & \alpha > 0 \\ 1, & \alpha = 0 \\ \displaystyle\int_{\alpha}^{t} (d\tau)^{\alpha}, & \alpha < 0 \end{cases} \tag{19} $$

where a and t are the limits of the FO operator, while α is the order of integration or differentiation ($\alpha \in \mathbb{R}$). Liouville-Riemann, Caputo, and Letnikov-Grunwald descriptions of FO calculus are the ones that are most often used in FO systems [54]. FO systems are differ from IO systems in their behavior, where FO systems may have roots in the right half s-plane and can be remain stable. The following equation can be used to represent the fractional-order LTI system

$$ \begin{aligned} &a_n D^{\alpha_n} y(t) + a_{n-1} D^{\alpha_{n-1}} y(t) + \cdots + a_0 D^{\alpha_0} y(t) \\ &= b_m D^{\beta_m} u(t) + b_{m-1} D^{\beta_{m-1}} u(t) + + \cdots + b_0 D^{\beta_0} u(t) \end{aligned} \tag{20} $$

The system (20), can then be reformulated with the equation (21)

$$ \sum_{k=0}^{n} a_k D^{\alpha_k} y(t) = \sum_{k=0}^{m} b_k D^{\beta_k} u(t) \tag{21} $$

The continuous model of the fractional-order system may be derived by applying the Laplace transform to (20) with zero initial conditions as follows

$$ G(s) = \frac{b_m s^{\beta_m} + \cdots + b_1 s^{\beta_1} + b_0 s^{\beta_0}}{a_n s^{\alpha_n} + \cdots + a_1 s^{\alpha_1} + a_0 s^{\alpha_0}} \tag{22} $$

where α_k, β_k ($k = 0, 1, 2, \ldots$) are real number, $\alpha_k < \alpha_{k-1} < \ldots < \alpha_0$, $\beta_k < \beta_{k-1} < \ldots < \beta_0$ and a_k, b_k ($k = 0, 1, 2, \ldots$) are random constants. To develop FO functions in real or simulation works, representation using IO transfer functions must be utilized. The Oustaloup's recursive transfer function is one of the common approximation tools, which utilizes recursive distribution of K constant, N zeros and N poles [54]. Thus, in this study, the higher-integer order filter is utilized for approximation of FO systems as expressed by Eq. (23)

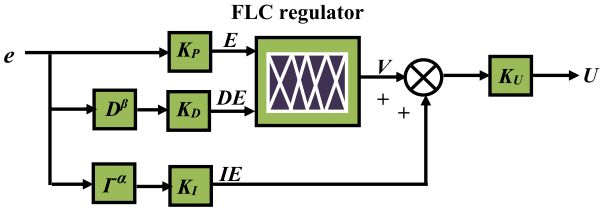

FIGURE 8. Schematic representation of FO-Fuzzy-PID regulator.

$$ s^{\alpha} \cong G_f(s) = K \prod_{k=-N}^{N} \frac{s + \omega_k'}{s + \omega_k} \tag{23} $$

where $\alpha \in (0, 1)$ represents the FO differintegration and N denotes the order of approximation. The constant K, the frequencies of the zeros ω_k and the poles ω_k' of the filter are determined from equations (24) and (25)

$$ \omega_k = \omega_l \left(\frac{\omega_h}{\omega_l}\right)^{\frac{K+N+\frac{1}{2}(1+\alpha)}{2N+1}}, \quad \omega_k' = \omega_l \left(\frac{\omega_h}{\omega_l}\right)^{\frac{K+N+\frac{1}{2}(1-\alpha)}{2N+1}} \tag{24} $$

$$ K = \omega_k^{\alpha} \tag{25} $$

where, ω_l and ω_h are the low and high frequencies bands [53]– [55]. In this article, the frequency band is utilized as $\omega = [10^{-3}, 10^{3}]$ rad/s, and the 5th order Oustaloup's recursive transfer function is exploited.

B. FO-FUZZY-PID REGULATOR

FO-Fuzzy-PID regulator exploited in this article has fractional-order Fuzzy PI and PD structures [56]. According to this concept, we developed a FO-Fuzzy-PID regulator for a PV-WFS application (Fig. 8). In this structure, their fractional counterparts amend the derivative operator of error (DE) at the input and integral (IE) at the output [57]. Under this arrangement, the integral action helps to remove the ultimate steady-state error.

In this diagram (Fig. 8), D^{β} is the fractional-derivative, and $I^{-\alpha}$ is the fractional-integrator order. The values of the fractional orders $\{\alpha, \beta\}$, along with the input–output coefficients $\{K_P, K_D, K_I, K_U\}$ of the considered regulator are the optimization parameters in the PSO process. For the proposed controller illustrated in Fig. 9, the fuzzy rule-bases can be formed using Mamdani method to exploit the nonlinearity impacts of fractional-operators and fuzzy mapping. The acting of all rule-bases produces the control signal (U) which is a nonlinear mapping function of the error E, DE and IE, as expressed in the basic equation (26):

$$ U(t) = \left(f\left(K_P e(t) + K_D \frac{d^{\beta}}{dt} e(t) \right) + K_I \frac{d^{-\alpha}}{dt} e(t) \right) K_U \tag{26} $$

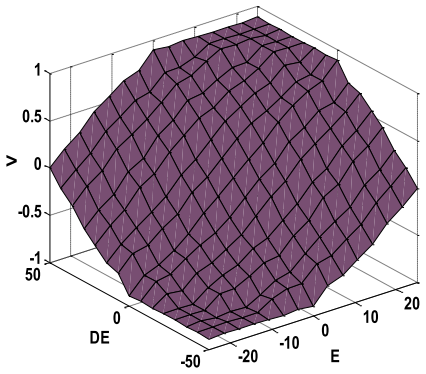

FIGURE 9. Rule-base for nonlinear control surface.

TABLE 4. The input/output variables and primary universes of the FO-Fuzzy-PID regulator.

Parameters	Type	Linguistic	Universe	
	I/O		Min	Max
System error (E)	Input	*LN MN SN ZE SP MP LP*	− 25	+ 25
Error change (DE)	Input	*LN MN SN ZE SP MP LP*	− 50	+ 50
Output control (V)	Output	*LN MN SN ZE SP MP LP*	− 1	+ 1

where, nonlinear function $f(.)$ is an input-output mapping of the FLC. Fig. 9 presents the nonlinear control surface of the determined fuzzy rule-bases.

Regarding the FLC principles, and according to the operation of the considered PV-WFS and the existing FO-Fuzzy-PID regulators, the fuzzy linguistic terms and the primary universes of the inputs/output are summarized in Table 4.

The input and output variables have seven linguistic terms (Table 4). The meta-rule of the rule-base is that **IF** the E and DE are both "Large" L and somewhat far from the reference **THEN** the V is "Large" L''. All of the membership functions (MFs) of the input and output variables use a triangular form, which is simple to compute and defines the complete fuzzy section of these variables.

The fuzzy linguistic expressions are defined as *LN*, *MN*, *SN*, *ZE*, *SP*, *MP*, *LP* where L, M, S, ZE, N, P, which denote large, medium, small, zero, negative, positive. Fig. 10 illustrates the fixed shaped MFs for the antecedents and consequents of the fuzzy inference. The primary universe of the input variables E and DE are standardized between $(-25, +25)$ and $(-50, +50)$, respectively. The primary universe of the output variable V is standardized between $(-1, +1)$.

The center of gravity technique can be utilized to determine the defuzzified output of the suggested FO-Fuzzy-PID regulator as:

$$U_f = \frac{\sum_{j=1}^{47} \gamma_j \mu_j}{\sum_{j=1}^{49} \mu_j} \tag{27}$$

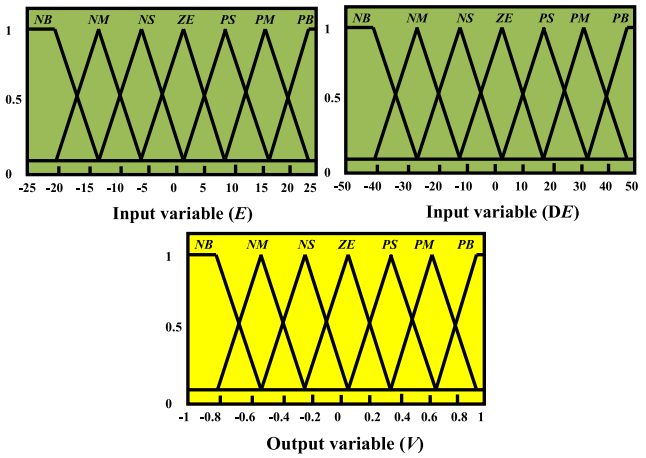

FIGURE 10. Fuzzy memberships for inputs/output.

where γ_j is a variable that contains the fuzzy output centroids of the output fuzzy membership (V). μ_j represents the membership grade in the outputs fuzzy set j.

The FO-Fuzzy-PID regulators perform better than the conventional PID controllers [56]. The important factor of the FO-Fuzzy-PID controller is the effectiveness of its performance, which is highly dependent on its tuning coefficients (i.e. K_P, K_D, K_I, K_U) and integral–differential orders $\{\alpha, \beta\}$. Due to the lack of precise data about PV-WFS model, the determination of these coefficients would not be optimal. As a result, the proposed FO-Fuzzy-PID regulator may not be able to provide good performance during the operating stages. This article proposes the best way to tackle this difficulty, in which the fractional-orders of the recommended FO-Fuzzy-PID regulator are optimized off-line with the fuzzy MFs scaling coefficients according to the operating conditions.

C. PROBLEM STATEMENT

The considered PV-WFS is a nonlinear system and has numerous goals. Effective implementation of the suggested control system needs optimization of design coefficients. Therefore, the first goal of this work is to design a meta-heuristic optimization algorithm (MOA)-based PSO methodology for the MPPT control of the zero-carbon energy source (ZCES)–based wire feeder system (WFS) while considering the fluctuation nature of ZCES. Moreover, the second objective is to use PSO algorithm for FO-Fuzzy-PID speed control system's design and perform the appropriately detailed analysis methods such as design procedure and dynamic analysis. In this article, the implementation of PSO algorithm paves the way for offline tuning of the control system parameters in the presence of PV energy resource and their variability consequences.

D. PSO METHOD

PSO method is a group intelligence nature-inspired population-based meta-heuristic search technique proposed

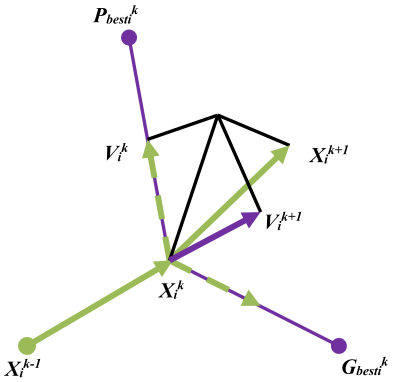

FIGURE 11. PSO searching process.

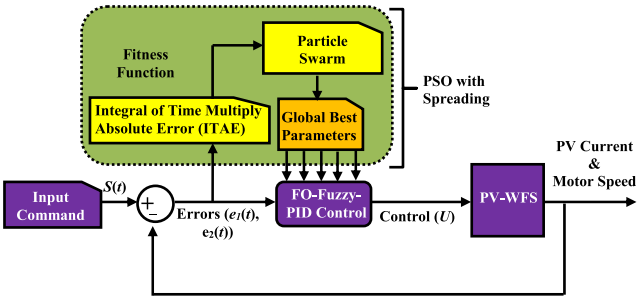

FIGURE 12. Actions of the optimization problem implemented by the PSO method.

by Kennedy to solve various mathematical problems [58]. PSO methods are exploited in many fields such as complex mathematical calculations, information science, automation, engineering, and other applications in the industrial world [56], [58]. Because PSO approach is an excellent optimization algorithm and a good strategy for determining the best regulator coefficients [41].

In light of the above discussion, PSO technique may be regarded a suitable strategy for searching best FO-Fuzzy-PID regulator coefficients. These metaheuristic techniques are started with an arbitrary distributed population $P = \{P_1, \ldots, P_n\}$ of the possible solutions, is often called '*swarm*'. The probable solutions $P_1, \ldots, P_n$ are called '*particles*'.

The PSO technique searches the full space of probable solutions, where the particles '*move*' to search for the overall best-fit solution 'G_{best}' [56]. Each entity has a position X_i^k and speed V_i^k related to it. The equations for updating the velocity and position of an entity 'i' are given by (28) and (29), respectively.

$$V_i^{k+1} = wV_i^k + c_1 r_1 \left(P_{best_i^k} - X_i^k\right) + c_2 r_2 \left(G_{best_i^k} - X_i^k\right) \tag{28}$$

$$X_i^{k+1} = X_i^k + V_i^{k+1} \tag{29}$$

where, c_1, c_2 are the acceleration-coefficients, P_{best} is the top location of particle, G_{best} is the top location of the group, r_1, r_2 are arbitrary variables equally distributed between 0 and 1, and w is the inertial weight calculated by Eq. (30)

$$w_k = w_{\max} - \left(\frac{w_{\max} - w_{\min}}{k_{\max}}\right).k \tag{30}$$

where w_{min} and w_{max} are the minimum and maximum values of inertial weight factor, and k_{max} is the maximum number of iterations. Updated position and velocity of the swarms for one iteration in PSO searching process are depicted in Fig. 11.

E. THE OPTIMIZATION PROBLEM

Through the design phase of a FO-Fuzzy-PID regulator, the parameter tuning process is turned into a multi-dimensional optimization problem, where both fractional-orders (α and β), and tuning coefficients of the fuzzy regulator (K_P, K_I, K_D, K_U) are observe as decision parameters. By this approach, the complexity of the optimization problem tends to produce multimodal error surfaces whose cost functions are extremely hard to reduce. Therefore, this article offers an approach for optimizing the parameter adjustment of the FO-Fuzzy-PID regulator. The optimization problem utilizes PSO technique to determine the parameters. The PSO tuning strategy entails determining the proper FO-Fuzzy-PID regulators coefficients for the regulation of PV-WFS with the best possible functionality. It performs offline search to obtain the most appropriate coefficients that leads to improved results in both dynamic and steady states. Fig. 12 presents the PSO method for the coefficients tuning operation of PV-WFS.

TABLE 5. Selection of parameters used for PSO-based adjusting of the FO-Fuzzy-PID regulator.

Parameter	Value
Number of iteration	100
Population size	50
Inertia weight	0.8
Cognitive weight	1.5
Social weight	1.5
Damping ratio	0.8
Sampling time	5e-5

All parameter values of PSO algorithm are given in Table 5. Under such conditions, the suggested PSO-based FO-Fuzzy-PID controller coefficients correspond to the dimensions of each possible solution for the optimization process.

The ITAE criterion was used in this study to determine the best solution with the shortest calculation time and highest accuracy, based in the instantaneous error of the PV generator current loop $e_1(t)$ and the instantaneous error in the motor speed loop $e_2(t)$. The ITAE index J evaluates the convergence between the closed-loop step response of PV current (I_{pv}) and PMDC motor speed (ω) produced by a specified coefficient design, and the input command function $S(t)$. Therefore, the merit of each proposed solution is evaluated according to the following cost function

$$J = J_1 + \lambda J_2 = \int_0^{t_{sim}} t\,|e_1(t)|\,dt + \lambda \int_0^{t_{sim}} t\,|e_2(t)|\,dt \tag{31}$$

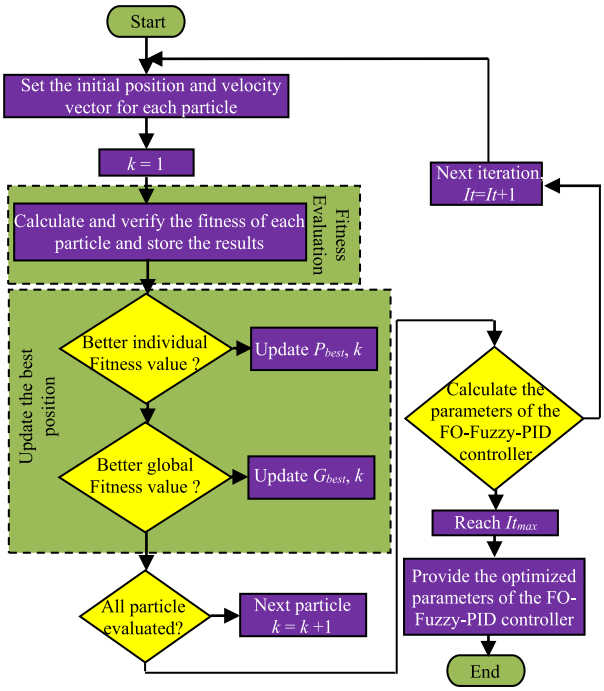

FIGURE 13. Schematic representation of the PSO method.

where λ is weighting coefficient and t_{sim} is the computational time. On the other hand, the difficulty of calibrating coefficients of PSO-base FO-fuzzy-PID algorithm for a PV-WFS can be defined as a twelve-factor restricted optimization problem, which comprises: K_{P1}, K_{P2}, K_{I1}, K_{I2}, K_{D1}, K_{D2}, K_{U1}, K_{U2}, α_1, α_2, β_1, β_2:

$$\begin{aligned} &Minimize\ J(x)x = (\alpha_1, \beta_1, K_{P1}, K_{I1}, K_{D1}, K_{U1}, \alpha_2, \beta_2, \\ &\qquad K_{P2}, K_{I2}, K_{D2}, K_{U2}) \in \Re^{12} \\ &Subject\ to:\ 0 \le \alpha_1, \beta_1, \alpha_2, \beta_2 \le 1; \\ &\qquad 0 \le K_{P1}, \quad K_{P2} \le 20; \\ &\qquad 0 \le K_{I1}, \quad K_{I2} \le 20; \\ &\qquad 0 \le K_{D1}, \quad K_{D2} \le 20; \\ &\qquad 0 \le K_{U1}, \quad K_{U2} \le 20 \end{aligned} \tag{32}$$

The operation of this cost function is determined depending to PSO method as illustrated in Fig. 13.

The optimization performance of the proposed PSO-based FO-Fuzzy-PID regulator is evaluated by plotting the optimal objective function values obtained from 100 iterations. The test results are depicts in Fig. 14. By analyzing Fig. 14, it can be found that the complete performance of the proposed PSO-based FO-Fuzzy-PID regulator is the best, followed by the PSO-based FLC regulator and the PSO-based FOPID regulator, and the worst is the PSO-based PID regulator. Within a certain number of iterations, PSO-based FO-Fuzzy-PID regulator (19 iterations), PSO-base FLC regulator (18 iterations), PSO-based FOPID regulator (77 iterations), and PSO-based PID regulator (80 iterations) can converge to the target precision.

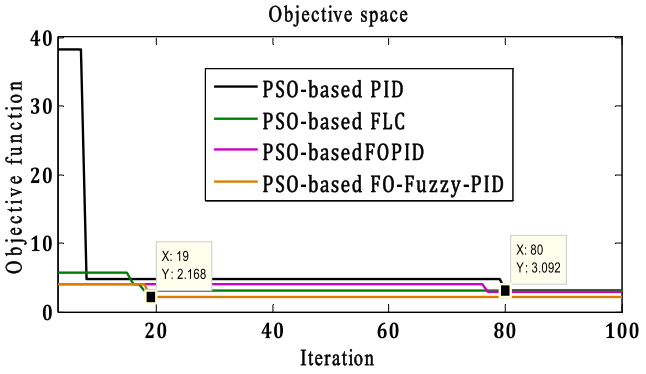

FIGURE 14. Convergence graph of the cost function of different regulators in 100 runs.

TABLE 6. Optimal regulator parameters obtained by PSO at 100 runs.

Algorithm	P&O MPPT Currant Control (D_1)	Wire Speed Control (D_2)
FO-Fuzzy-PID	K_{P1}=10.20; K_{I1}=8.60; K_{D1}=0.31; K_{U1}=5.22;α_1=1.31; β_1=1.01	K_{P2}=15.33; K_{I2}=12.31; K_{D2}=0.14; K_{U2}=3.65; α_2=1.22; β_2=1.91
FOPID [22]	K_{P1}=11.7; K_{I1}=9.52; K_{D1}=0.17; α_1=1.20; β_1=1.65	K_{P2}=13.07; K_{I2}=10.48; K_{D2}=0.30;α_2=1.73; β_2=1.80
PID	K_{P1}=8.11; K_{I1}=4.95; K_{D1}=0.10;	K_{P1}=13.3;K_{I1}=16.6;K_{D1}=0.2
FLC [59]	K_e=0.15; K_Δ=0.10; K_z=10	K_e=0.01; K_Δ=0.05;K_z=20

TABLE 7. Statistical results obtained data of diverse regulators in 100 runs.

Control	Fitness function			Convergence time (hour)			Iteration number of convergence		
	max.	min.	mean	max.	min.	mean	max.	min.	mean
FO-Fuzzy-PID	4.03	2.16	3.09	0.31	0.09	0.20	19	15	17
FLC	5.66	3.03	4.34	0.29	0.04	0.16	18	14	16
FOPID	4.05	2.90	3.47	0.48	0.20	0.34	77	63	70
PID	38.16	3.09	20.6	0.56	0.25	0.40	80	68	74

As a result, the global search ability of the suggested PSO-based FO-Fuzzy-PID regulator is stronger, the convergence speed and convergence precision are higher. However, the proposed PSO-based FO-Fuzzy-PID regulator still performs poorly when iterating to 100 times. Therefore, the efficacy of the suggested regulator in this paper is proved.

The optimum solution values of the respective gains and proportional, integral and differential values are reported in Table 6, and quantitative results are provided in Table 7. From Table 7, it is obvious that the suggested regulator has the lowest fitness function compared to other regulators due to fractional-order and fuzzy mechanisms, which give it superior performance over other regulators.

IV. CONTROL DESIGN OF THE PROPOSED MPPT ALGORITHM

As multiple power points exist in (V_{pv}–I_{pv}) and (P_{pv}–V_{pv}) characteristics of a solar PV generator, It is essential that the solar PV generator provide maximum power all the time. Different MPPT methods have been reported for PV systems

[49]. Among all the MPPT method, P&O is the most basic and most famous algorithm in the determination of the MPP for a solar PV generator due to generality, i.e. validity for any PV system, and simplicity of implementation [60].

The amount of voltage and current at MPP of the PV generator for all the steps of the P&O MPPT method are changed with a constant variable in P&O MPPT method. However, this variable is caused by oscillation at MPP of the P&O MPPT algorithm. Compared to traditional P&O MPPT algorithms, it is shown in Dhaker *et al.* [49] that an enhanced P&O based MPPT method can follow the MPP quickly and properly under variable environmental conditions, such as irradiance and temperature.

Therefore, this paper combines FO-Fuzzy-PID current regulator with an enhanced P&O MPPT method to enhance the PV generator performance. The basic principle of the improved P&O MPPT algorithm is to increase step-variation to converge more rapidly to the MPP, while minimizing oscillations [49].

Really, to track quickly, increment-step 'H' is minimized or adjusted from one area to another: $H = 0.01$ in "X" zone and $H = 0.001$ in "Y" zone (Fig. 15). The procedure to generate the PV reference current (I^*_{pv}) is as follows. The inputs to the improved P&O MPPT method are PV voltage (V_{pv}), PV current (I_{pv}), and PV power (P_{pv}), respectively. The improved P&O MPPT block has an increment-step called (H) which changes from one zone to another, with values ranging from 0.001 to 0.01. The improved (P&O) MPPT method is developed as follows:

Step 1: The starting values for the PV power (P_{pv}), PV voltage (V_{pv}), and PV current (I_{pv}) are calculated.

Step 2: If the change in P_{pv} is greater than the amount of coefficient (R); ($|dP_{pv}| > R$) and if the change in t P_{pv} is equal to zero ($P_{pv}(k) - P_{pv}(k-1) = 0$), then the initial PV current ($I_{pv}(k)$) is considered as the reference PV current ($I_{pv}(k) = I^*_{pv}$) or else, it is the difference or sum between the initial PV current and increment-step ($I^*_{pv} = I_{pv}(k) + H$).

Step 3: If the change in P_{pv} is higher than Zero ($P_{pv}(k) - P_{pv}(k-1) > 0$) and if the difference in the PV voltage is greater than zero ($V_{pv}(k) - V_{pv}(k-1) > 0$), then the reference PV current is the difference between initial PV current and increment-step ($I^*_{pv} = I_{pv}(k) - H$) or else, it is the sum of the PV initial current and increment-step ($I^*_{pv} = I_{pv}(k) + H$).

Step 4: If the change in P_{pv} is lower than Zero ($P_{pv}(k) - P_{pv}(k-1) < 0$) and if the change in the PV voltage is greater than zero ($V_{pv}(k) - V_{pv}(k-1) > 0$), then the reference PV current is the difference of initial PV current and increment-step ($I^*_{pv} = I_{pv}(k) - H$) or else, it is the sum of the initial PV current and increment-step ($I^*_{pv} = I_{pv}(k) + H$). Fig. 16 illustrates the graphical representation for the improved P&O MPPT method.

Fig. 17 depicts the control system of the considered two-stage approach for an improved P&O-based MPPT method with an optimized FO-Fuzzy-PID regulator. The control scheme is composed of two loops: the primary is based on an improved P&O MPPT method for calculating the reference

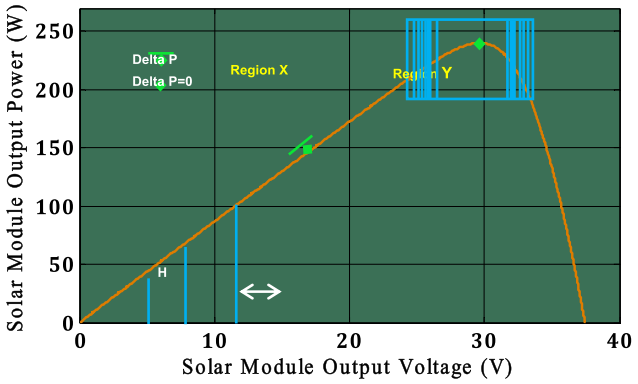

FIGURE 15. Basic principle of the enhanced (P&O) MPPT algorithm with an adaptive step increment [49].

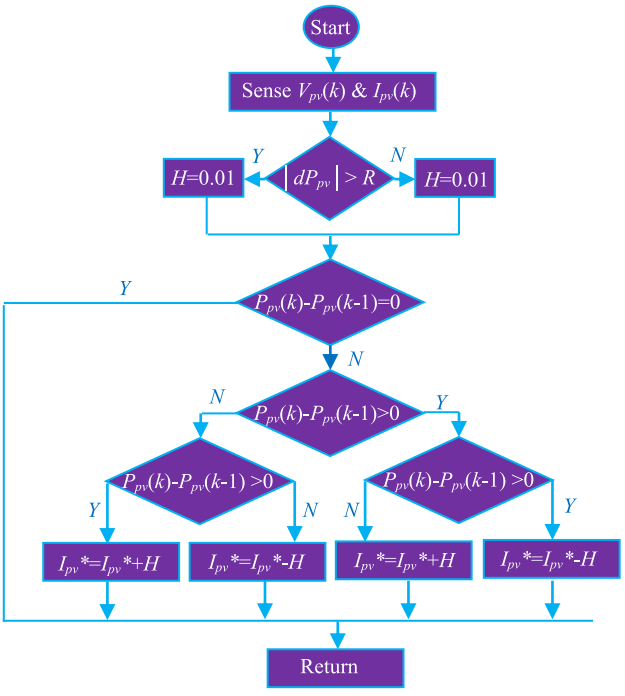

FIGURE 16. The graphical representation of the improved (P&O) MPPT method [49].

PV current, while the second is for MPP tracking. The V_{pv} and I_{pv} are received from PV generator and transmitted to the P&O MPPT searching technique to produce the reference current I^*_{pv}. Then, the duty ratio of the DC/DC buck converter is adjusted by the PSO and FO-Fuzzy-PID-tuned P&O MPPT regulators to extract the maximum possible power from the PV generator. These proposed algorithms tracks I^*_{pv} and generates minor fluctuations in the region of the MPP.

V. CONTROL DESIGN FOR WIRE FEEDER SYSTEM

The performance of the wire feeder regulator is critical, due to the fact that arc welding equipment must be able to feed welding wire at high rates in a few milliseconds when working collectively with the PMDC servo motor in the welding WFS system. In order to track the specified welding wire velocity,

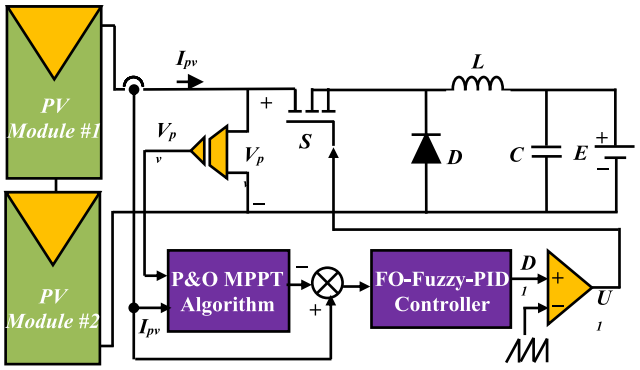

FIGURE 17. Control mechanism of FO-Fuzzy-PID current-controlled P&O method.

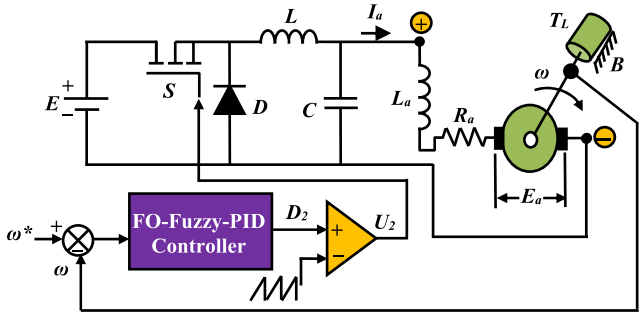

FIGURE 18. FO-Fuzzy-PID speed regulation of a PMDC motor in the welding WFS system.

the wire feeder regulator must have a high dynamic performance. The fluctuations in torque demand are large because, for example, a 400 ampere rated arc welding regulator must create welding connections with electrodes ranging in diameter from 0.6 mm to 1.6 mm. On the other hand, the material composition of the welding wire (or consumable electrode) can also differ greatly. Therefore, for precise wire feed speed tracking, the PMDC servo motor requires an efficient and consistent speed regulator. This section suggests a high-speed feeding control method for the welding WFS to achieve welding quality. Moreover, the proposed PSO based FO-Fuzzy-PID regulator is utilized to achieve the control goals as far as possible by applying an adequate necessary duty ratio to the second DC/DC buck converter. Fig. 18 depicts an integrated mechanical system for implementing the considered welding wire feeder regulator. As seen in this figure, the welding WFS system is divided into 3 components: a sola PV generator with a constant power source (E), PMDC servo motor, and a PSO-based FO-Fuzzy-PID speed regulator. The wire electrodes must be fed constantly via the welding WFS system from the wire spool to a welding gun at a fixed speed during a welding operation. To this end, a PMDC motor integrated into the welding WFS system rotates at a constant speed; the latter is normally set in the range 10–150 rad/s during the welding process.

VI. SIMULATION RESULTS AND DISCUSSIONS

Extensive closed-loop simulations were performed using MATLAB/SIMULINK tool for the proposed PV-WFS. Simulation diagram of the PV modules powered PMDC motor

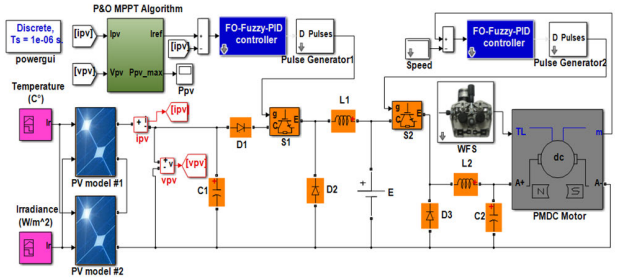

FIGURE 19. Simulation diagram of the PV modules powered PMDC motor for welding WFS.

for welding WFS application is illustrated in Fig. 19. The comparative simulation of the algorithms includes PSO-based FO-Fuzzy-PID presented in this article, PSO-based FOPID [59], PSO-based FLC [60], and PSO-based basic PID regulator. In the simulation, five tests were conducted to show the tracking ability of the proposed PSO-based FO-Fuzzy-PID P&O MPPT method at various irradiance. In addition, a brief discussion of the PMDC motor performance is also provided for PSO-based FO-Fuzzy-PID speed control. So, the simulation was performed five times for each examination. The first test was to show PV-WFS behavior at a fixed and homogeneous amount of solar irradiation. The second test was to demonstrate the response of the PSO-based FO-Fuzzy-PID P&O MPPT regulator for ramp-change in the irradiation level. The third test aimed at assessing the PV-WFS performance in step-change in radiation value. The fourth test verified the performance of the proposed PSO-based FO-Fuzzy-PID P&O MPPT under partial shading conditions. The last test was to confirm the effectiveness and validity of the suggested PSO-based FO-Fuzzy-PID P&O MPPT under real solar irradiance and temperature during the testing day, which was a sunny and clear day.

A. PERFORMANCE TEST UNDER CONSTANT SOLAR RADIATION LEVEL

In case I, the PV-WFS system was simulated with uniform and constant radiation level ($G = 500$ W/m^2). The waveforms of the PV power for FO-Fuzzy-PID, FLC, FOPID, and PID-based P&O MPPT techniques are plotted in Fig. 20(a), and a zoom-in these results is presented in Fig. 20(b). It can be seen from Figs. 20(a) and (b) that the PV power is fluctuates between 480.48 and 480.49 W for the suggested FO-Fuzzy-PID-based P&O MPPT method. The fluctuation in PV power is 16.20 W at the MPP for the PID based P&O MPPT technique, whereas the FLC based P&O MPPT method provides a smaller content of ripple estimated at 0.020 W (Fig. 20(c)). In the transient state, the FOPID regulator -based P&O MPPT technique takes 0.0869 s to achieve its MPP, while the PID-based P&O MPPT technique reaches the MPP in 0.1573 s. The settling-time achieved by the suggested FO-Fuzzy-PID-based P&O MPPT method is 0.0427 s. The PV curves illustrate that the suggested FO-Fuzzy-PID

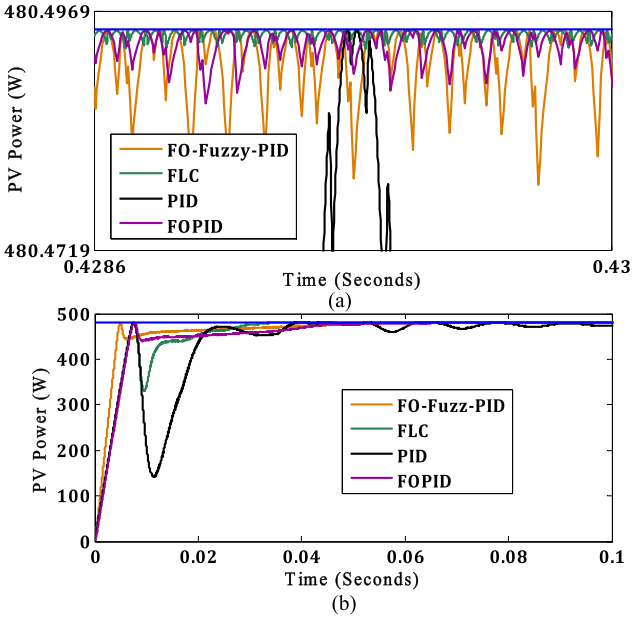

FIGURE 20. Performance for case I on application FO-Fuzzy-PID, FLC, FOPID and PID regulator based P&O MPPT techniques: (a) output powers, (b) zoom in the output powers.

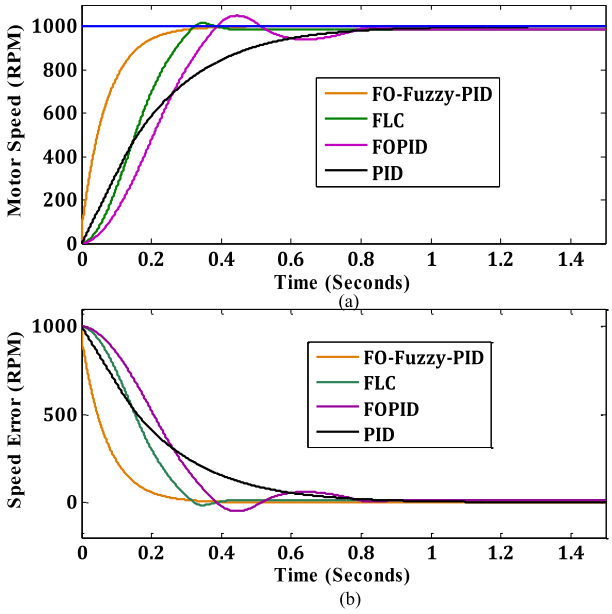

FIGURE 21. Performance for case I on implementing FO-Fuzzy-PID, FLC, FOPID and PID based velocity regulation of PMDC motor: (a) motor speeds, (b) speed errors.

TABLE 8. Comparative performance study of P&O MPPT method for the case I.

Radiation and Temperature	P&O MPPT	V_{pv} (V)	I_{pv} (A)	η_{MPPT} (%)	t_{sMPP} (s)	P_{loss} (W)
500W/m^2, 25°C	FO-Fuzzy-PID	58.40	7.92	96.35	0.042	17.53
	FLC	59.30	7.64	94.29	0.040	27.43
	FOPID	58.78	7.80	95.43	0.086	21.95
	PID	57.07	7.73	91.82	0.157	39.30

and FLC regulator -based P&O MPPT methods outperform FOPID and PID-based P&O MPPT strategies. Table 8 summarizes the outcome of the comparison of the four regulators.

The following formula was utilized to calculate the MPPT tracking efficiency (32)

$$\eta_{\text{MPPT}} = \frac{\int_0^t P_{\text{real}}(t)dt}{\int_0^t P_{\text{max}}(t)dt} \tag{33}$$

where P_{real} and P_{max} are the solar PV modules' actual and maximum power, respectively.

In case I, the proposed FO-Fuzzy-PID speed regulator allows the PMDC motor to track the desired speed of 1000 rpm within a very short time (0.40 s) compared to FLC, FOPID, and PID speed regulators, which take 0.93, 1.08, and 1.15 s, respectively (Fig. 21(a)). The speed control based on the FOPID regulator exhibits a strong oscillation characteristic and very slow reaction time. Also, the suggested regulator outperforms the FLC, FOPID, and PID in closed-loop speed regulation, because of the nonlinear nature of the PMDC motor. The steady-state error is negligible for all four control schemes, as shown in Fig. 21(b).

B. PERFORMANCE INVESTIGATION UNDER RAMP-CHANGE IN RADIATION VALUE

The irradiance profile applied in test II is depicted in Fig. 22(a). Irradiance is changed linearly from 100 W/m^2 to 1000 W/m^2 and then from 1000 W/m^2 to 100 W/m^2 at 25 °C and the resulting data is examined. The PV power (P_{pv}) is maintained at MPP by using the suggested FO-Fuzzy-PID control-based P&O MPPT technique, despite the variation in irradiance (Fig. 22(b)). High ripple content in MPP can be observed when PID control-based P&O MPPT technique is implemented, as depicted in Fig. 22(b) and (b). The PID-based P&O MPPT method causes a very large ripple content estimated at 10.40 W, while the FLC-based P&O MPPT method only delivers 0.05 W. For the FOPID based P&O MPPT technique, it produces a maximum power ripple of 0.03 V. Finally, the suggested FO-Fuzzy-PID based P&O MPPT method minimizes the power ripple to 0.005 W and offers a settling time of 0.001 s to attain MPP in the transient state for 0.1–0.3 s compared to 0.0823 s and 0.0945 s for FLC based P&O and FOPID based P&O MPPT, respectively.

In case II, the desired value of the motor velocity is increased from 500 to 1000 rpm (Fig. 23). The PMDC motor obtains its reference speed rapidly with negligible overshoot when the suggested FO-Fuzzy-PID regulator is implemented. From Fig. 23, one can see that the peak overshoot is completely eliminated with the proposed FO-Fuzzy-PID and PID regulator.

In contrast, it is 11.45% and 9.35% for FOPID and FLC regulators, respectively. Furthermore, the settling time is reduced from 0.8 s with PID regulator to 0.2 s with FO-Fuzzy-PID regulator. The comparative performance of PMDC motor

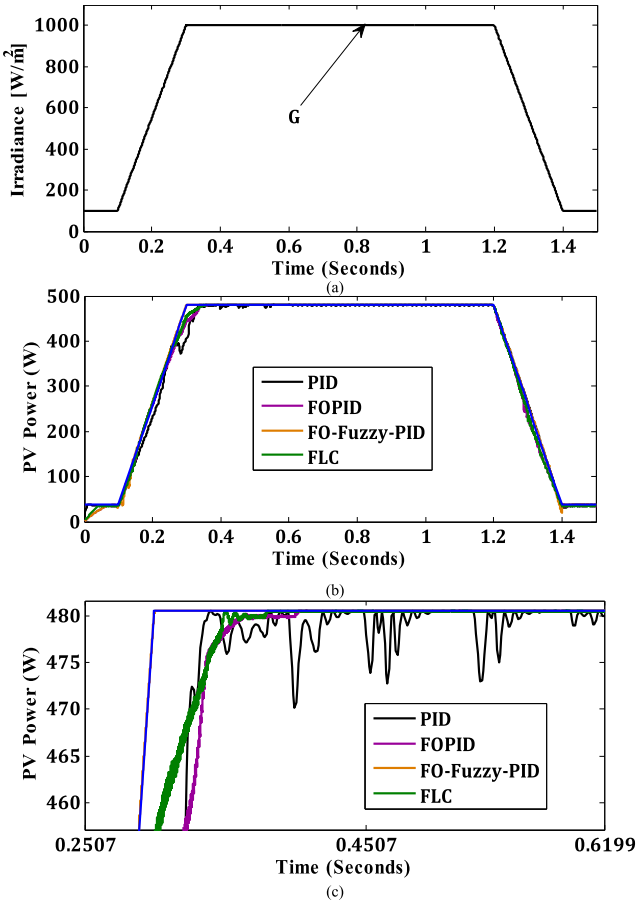

FIGURE 22. Performance for case II on implementing FO-Fuzzy-PID, FLC, FOPID and PID regulator based P&O MPPT techniques: (a) irradiance profile, (b) output powers, (c) zoom in the output powers.

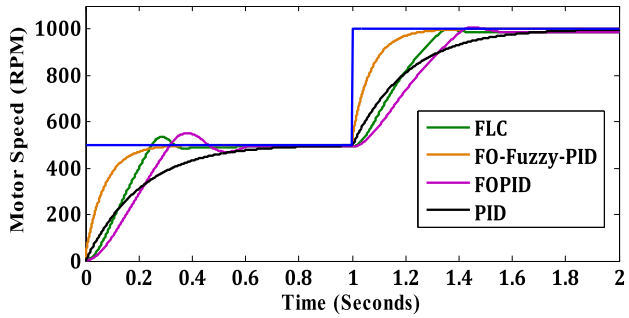

FIGURE 23. Performance for case II on implementing FO-Fuzzy-PID, FLC, FOPID and PID based speed regulation of PMDC motor.

verifies the improved results of the proposed PSO based FO-Fuzzy-PID speed regulator.

C. PERFORMANCE INVESTIGATION UNDER GRADUAL -CHANGE IN RADIATION VALUE

In test III, the PV-WFS is tested with a gradual-change in solar irradiation level to mimic a quickly changing irradiation situation, so that the level of solar irradiation varies randomly at an interval of 0.15s and the results are recorded for evaluation. For serious analysis, three successive step changes are made in solar radiation levels.

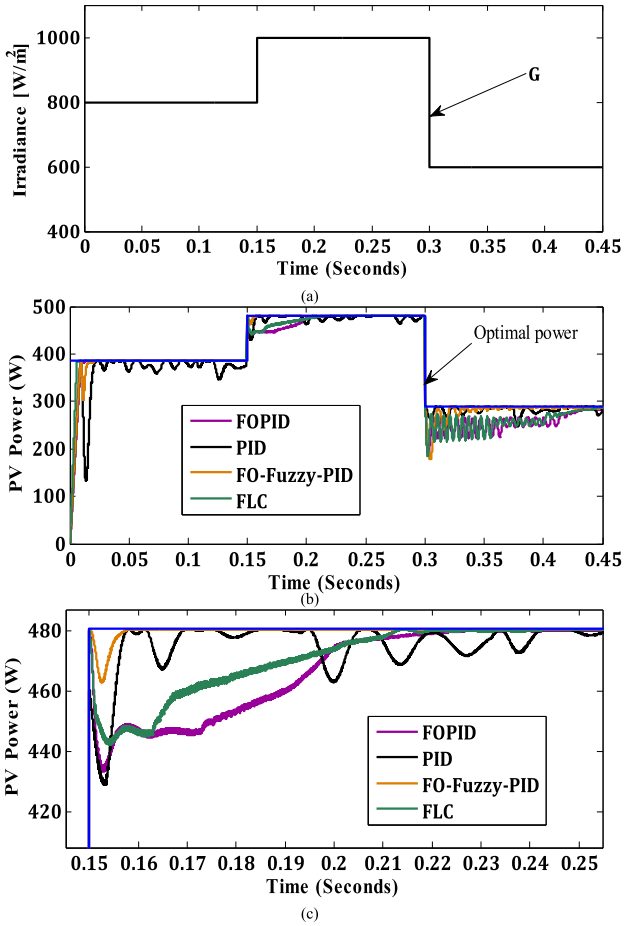

FIGURE 24. Performance for case III on implementing FO-Fuzzy-PID, FLC, FOPID and PID regulator based P&O MPPT techniques: (a) irradiance profile, (b) output powers, (b) zoom in the output powers.

As depicted in Fig. 24(a) the value of radiation is quickly changed from 800 to 1000 W/m^2, then, rapidly decreased to 600 W/m^2. Figs. 24(b) and 24(b) illustrate the waveforms for step-change in radiation value. As depicted in these figures, during interval time 0.15 to 0.25 s, the system takes 0.1 s to stabilize around the MPP with an efficiency of 96.83% for the PID regulator based P&O MPPT method.

In addition, the power ripple is $>$ 33.10 W, which leads to high oscillations around the MPP. The efficiency of the suggested FO-Fuzzy-PID regulator based P&O MPPT method is round 98.95%, with response time $<$ 0.02 s, and a power ripple $<$ 0.8 W.

The FLC and FOPID regulators take longer to attain the MPP in the situation of gradual variation in solar irradiation. The efficiency of this system in this test is low with the FLC and FOPID regulators, which is 95.10% and 93.25%, respectively. Hence, under this scenario, the proposed FO-Fuzzy-PID regulator based on the P&O MPPT method presents a faster response with good efficiency and negligible power oscillations. A comparison of the four regulators performance is presented in Table 9 for case III.

TABLE 9. Performances investigation of the four compared MPPT methods for case III.

Irradiance and Temperature	P&O MPPT	η_{MPPT} (%)	t_{sMPP} (s)	P_{loss} (W)
800 W/m2, 25°C	FO-Fuzzy-PID	98.12	0.018	7.26
	FLC	97.07	0.014	11.32
	FOPID	95.61	0.019	16.96
	PID	89.55	0.037	40.38
1000 W/m2, 25°C	FO-Fuzzy-PID	98.95	0.013	05.04
	FLC	95.10	0.081	23.54
	FOPID	93.25	0.094	32.43
	PID	96.83	0.100	15.23
600 W/m2, 25°C	FO-Fuzzy-PID	96.41	0.045	10.38
	FLC	87.36	0.138	36.55
	FOPID	85.74	0.152	41.23
	PID	93.96	0.147	17.46

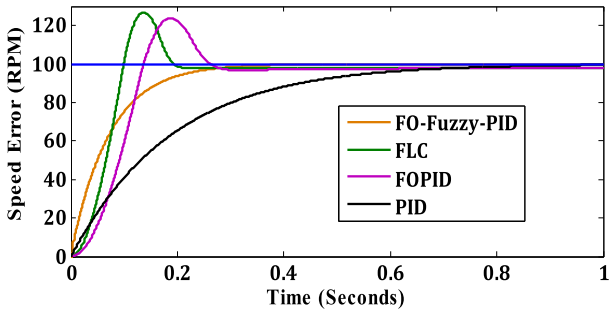

FIGURE 25. Performance for case III on implementing FO-Fuzzy-PID, FLC, FOPID and PID based velocity regulation of PMDC motor.

TABLE 10. Performances comparison of FO-Fuzzy-PID, FLC, FOPID and PID velocity regulation of PMDC motor for case III.

Regulator type	Rise time (s)	Settling time(s)	Overshoot (%)	Pick time(s)
FO-Fuzzy-PID	0.1686	0.3875	-	-
FLC	0.0931	0.5732	26.7	0.1372
FOPID	0.1274	0.6691	23.5	0.1877
PID	0.5008	0.9458	-	-

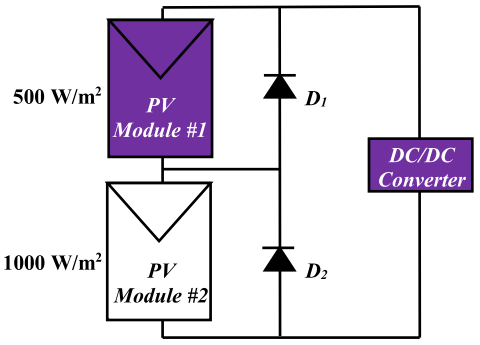

FIGURE 26. Irradiance on PV panels in test scenario.

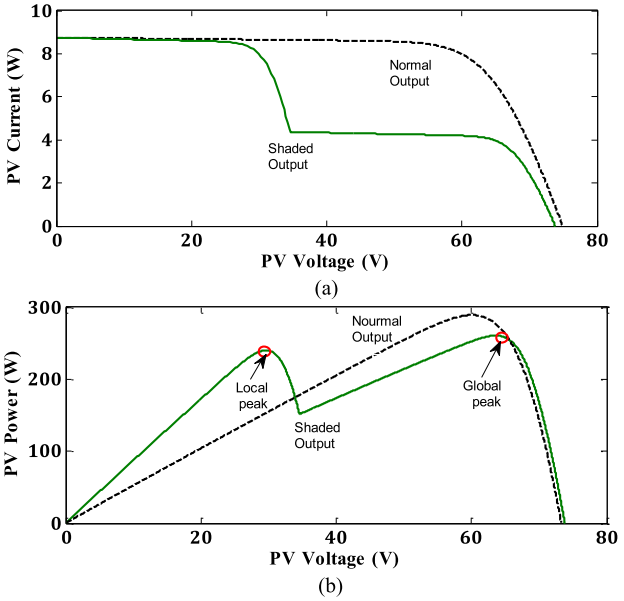

FIGURE 27. Response of PV panels: (a) the (P_{pv}–V_{pv}) characteristic under PSC. (b). the (I_{pv}–V_{pv}) characteristic under TSC.

In case III, the considered FO-Fuzzy-PID regulator exhibited much better speed response than the PID, FLC and FOPID regulators (Fig. 25), in all the aspects utilized as criterion for assessing the performance of transient response, and also in the steady state error. In term of rise time for example, the considered regulator created a response that was almost three times quicker than the PID regulator. The proposed FO-Fuzzy-PID also created the same style in terms of maximum overshoot, peak time, and steady state errors. Despite the fact that the FLC and FOPID regulators appeared to have somewhat superior speed responses than the PID regulator, both control schemes presented the same weaknesses in maximum overshoot. Table 10 lists the performance of PMDC Motor with four regulators for case III.

D. PERFORMANCE TEST UNDER TOP SHADING CONDITION (TSC)

In case IV, the standalone PV-WFS was tested with top PV panel shaded. The solar PV generator was irradiated with 500 W/m^2 at top. The irradiance considered for top shading condition (TSC) of the PV panels is shown in Fig. 26. A bypass diode is circuited across the top PV panel to make the current flow from the un-shaded PV panel to get around this condition. Because of this link of bypass diodes there will be multiple peaks formation in (P_{pv}-V_{pv}) curve. Fig. 27(a) and Fig. 27(b) show the power against voltage (P_{pv}-V_{pv}) and current against voltage (I_{pv}-V_{pv}) plots under TSC for the system under study together with the standard output (P_{pv}-V_{pv}) and (I_{pv}-V_{pv}) curves obtained at 1000 W/m^2 irradiance and 25 °C of temperature. In these figures, the MPP of the PV generator may decrease significantly and the (P_{pv}-V_{pv}) characteristic contains two peaks (global and local MPPs). In Fig. 28, the suggested FO-Fuzzy-PID based P&O MPPT method is compared with other regulators under TSC. In this situation, the global maximum peak power (260.85 W) was tracked by the suggested FO-Fuzzy-PID based P&O MPPT method under TSC. Otherwise, the PID based P&O MPPT method gives the lowest amount of power.

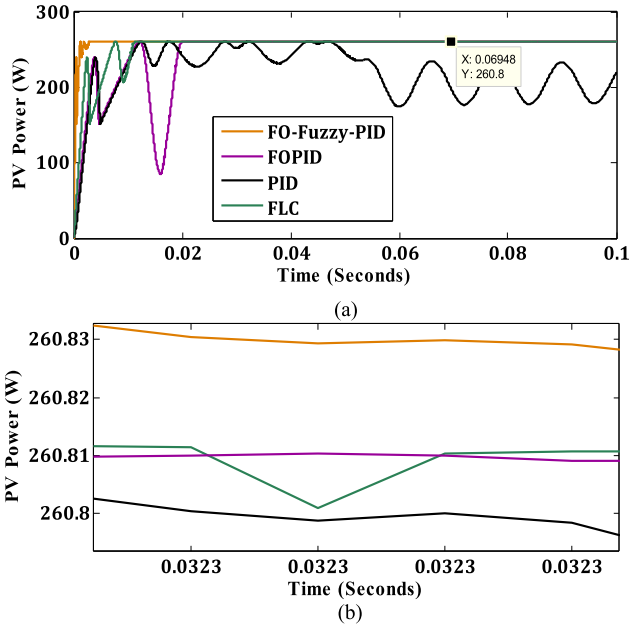

FIGURE 28. Performance for case IV on implementing FO-Fuzzy-PID, FLC, FOPID, and PID regulator based P&O MPPT techniques: (a) output powers, (b) zoom in the output powers.

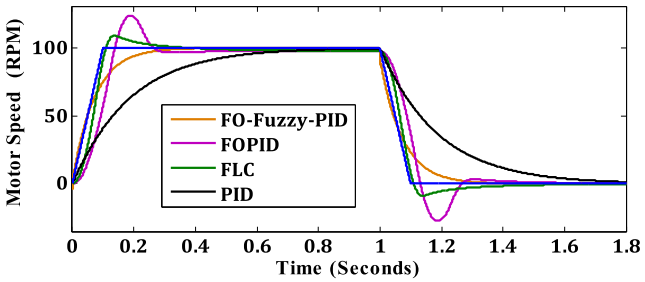

FIGURE 29. Performance for case IV on implementing FO-Fuzzy-PID, FLC, FOPID and PID based velocity regulation of PMDC motor.

TABLE 11. Performances comparison of the simulated speed regulators.

Parameters	FO-Fuzzy-PID	FLC	FOPID	PID
Rise time (s)	0.1793	0.1003	0.1301	0.4822
Steady state error (rpm)	0.001	2.07	2.24	0.65
Overshoot (rpm)	-	9	23.61	-
Settling time (s)	0.340	0.65	0.85	0.92

In case IV, the PMDC motor response under ramp-change in reference speed is obtained. The speed response for different regulators is depicted in Fig. 29, which indicates the capability of the proposed FO-Fuzzy-PID regulator to reduce the system overshoot compared to FLC and FOPID speed regulators. Moreover, with the proposed regulator, the real speed reaches the desired speed quickly (0.34 s). The settling time is about 0.65, 0.85, and 0.92 s for FLC, FOPID and PID speed regulators, respectively. Hence, the proposed FO-Fuzzy-PID regulator can provide sufficient speed tracking compared to other speed regulators. From the obtained responses, a variety

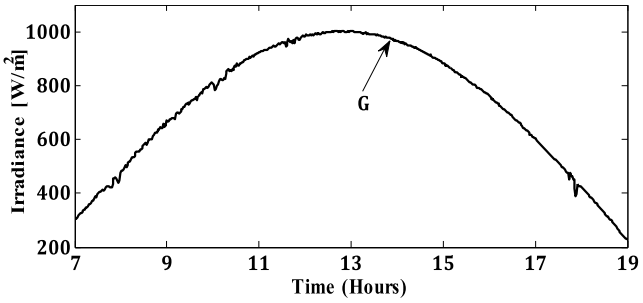

FIGURE 30. Solar radiation curve during the testing day.

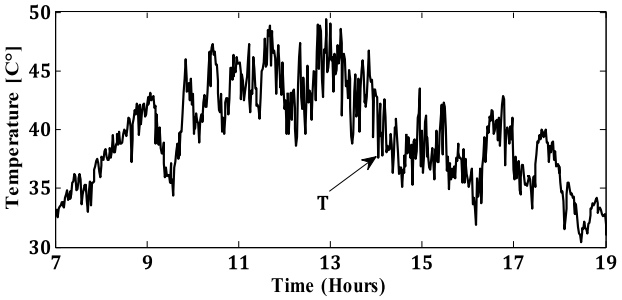

FIGURE 31. Ambient temperatures during the testing day.

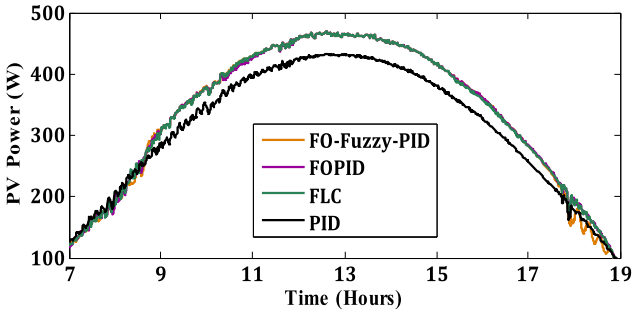

FIGURE 32. Performance for case V on implementing FO-Fuzzy-PID, FLC, FOPID and PID regulator based P&O MPPT techniques.

of parameters were measured to assess the performance of the PMDC motor (Table 11).

E. PERFORMANCE TEST UNDER REAL CLIMATIC DATA (RCD)

In case V, the FO-Fuzzy-PID based P&O MPPT method is evaluated under RCD in Sétif, Algeria. Fig. 30 and Fig. 31 show solar radiation and ambient temperature curves during the testing day (07:00 am – 19:00 pm), which was a sunny and clear day (30 July 2020). Fig. 32 shows the results obtained by the four regulators based P&O MPPT method under RCD. This figure demonstrates the potential and superiority of the proposed FO-Fuzzy-PID based P&O MPPT method over FLC, FOPID, and PID based P&O MPPT method.

For greater understanding, the hourly efficiency (HE) is computed. This variable comprises of the average power delivered per hour against the PV generator maximum output

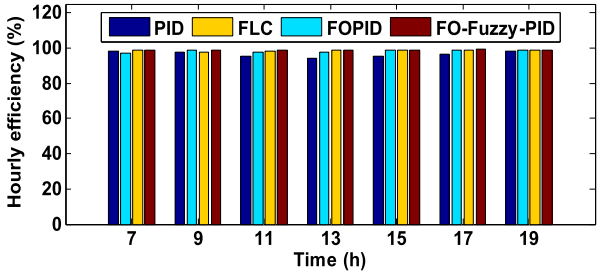

FIGURE 33. Measured hourly efficiency of solar the PV-WFS for the four MPPT regulators.

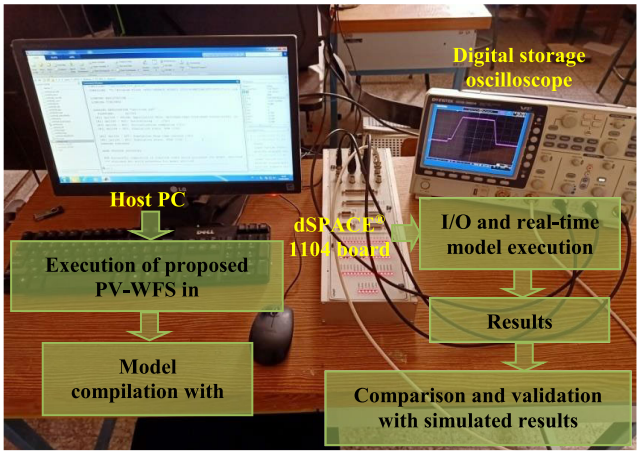

FIGURE 34. Real-time HIL testing platform of the proposed FO-Fuzzy-PID regulator.

power (P_{pv}-optimal). The *HE* formula for a PV generator can be defined as in [61]:

$$HE = \frac{\sum_{k=1}^{N} P_{\mathrm{MPP}}(k)/\mathrm{N}}{P_{\mathrm{pv\_optimal}}(t)} \tag{34}$$

where N represents the number of samples per hour.

The bar-chart in Fig. 33 provides a comparison of the HE. For this case, the efficiency of the proposed regulator is better with RCD than the other P&O MPPT regulators.

F. COMPARATIVE ANALYSIS AND DISCUSSIONS

Table 12 records the best-found regulator structure from the simulations in a tabular representation. It is clear that the suggested FO-Fuzzy-PID regulator outperforms the others in almost all evaluation criteria such as the average generated power, the efficiency and the power fluctuations. However, when compared concerning convergence time, the FLC regulator case gives in some better results. Moreover, the FO-Fuzzy-PID regulator has a high implementation difficulty, and its effectiveness heavily reliant on human expertise in designing the suitable control rules and membership functions. Furthermore, choosing the proper initial scaling coefficients of FO-Fuzzy-PID regulator is difficult due to the six initial parameters (K_P, K_I, K_D, K_U, α, β) that were adjusted. These coefficients need to be properly adjusted; otherwise, the effectiveness of the considered MPPT regulator can be significantly influenced.

TABLE 12. Summary of best regulator performances to meet different control objectives.

Parameters evaluation	Irradiance and temperature	FO-Fuzzy-PID	FOPID	FLC	PID
Mean power(W)	(Case I)	480.25	480.33	480.45	476.25
Efficiency (%)	G=500	96.35	95.43	94.29	91.82
Power ripples(W)	W/m^2	Neglected	Neglected	Neglected	16.20
Settling time ts(s)	T=25°C	0.0427	0.0869	0.0408	0.1573
Mean power(W)	(Case III)	285.34	247.30	249.50	274.72
Efficiency (%)	G=600	96.41	85.74	87.36	93.96
Power ripples(W)	W/m^2	Neglected	41.70	48.80	13.75
Settling time t_s(s)	T=25°C	0.045	0.152	0.138	0.147
Implementation complexity	-	High	Medium	High	Low
Depending on the model of the system	-	Not obligatory	Obligatory	Not obligatory	Obligatory
Methodology of control	-	Intelligent control	Sampling method	Intelligent control	Sampling method
Parameters for initialization	-	06 Parameters	06 Parameters	03 Parameters	03 Parameters

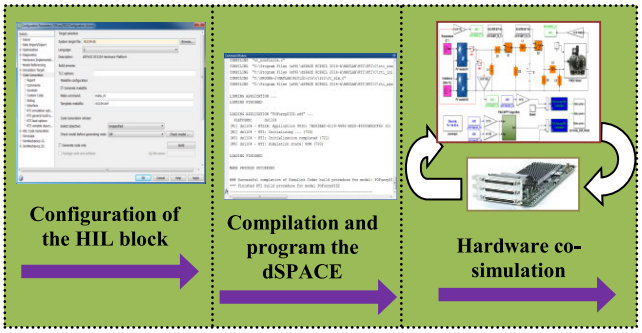

FIGURE 35. HIL test main block diagram.

G. EXPERIMENTAL VALIDATION

The considered optimal PSO-based FO-Fuzzy-PID control algorithms were experimentally validated on a PV-WFS prototype including dSPACE®1104 processor board to further confirm the analysis and simulation results. A photograph of the experimental prototype hardware is depicted in Fig. 34. Installing physical test schemes for PV-WFS requires a large, costly, and highly experienced technical team to coordinate the networking activities and keep detailed inventories of hardware. With technological advancements, physical test systems have been replaced with a real-time HIL testing platform. The real-time HIL simulator validates system response in real-world scenarios and has become an essential tool for electrical system design and development.

H. HIL TEST, RESULTS, AND DISCUSSION

The HIL test is performed as described in the main block diagram presented in Fig. 35. In HIL experimentation, the dSPACE processor board is physically connected to the PV-WFS model executing in the MATLAB/Simulink environment. The processor board contains a dual-core processor TMS320F379D, which is programmed in the MATLAB/Simulink environment using the fast prototyping approach. Discrete representations of the mentioned regulators are created from Simulink, and the output or hex file is

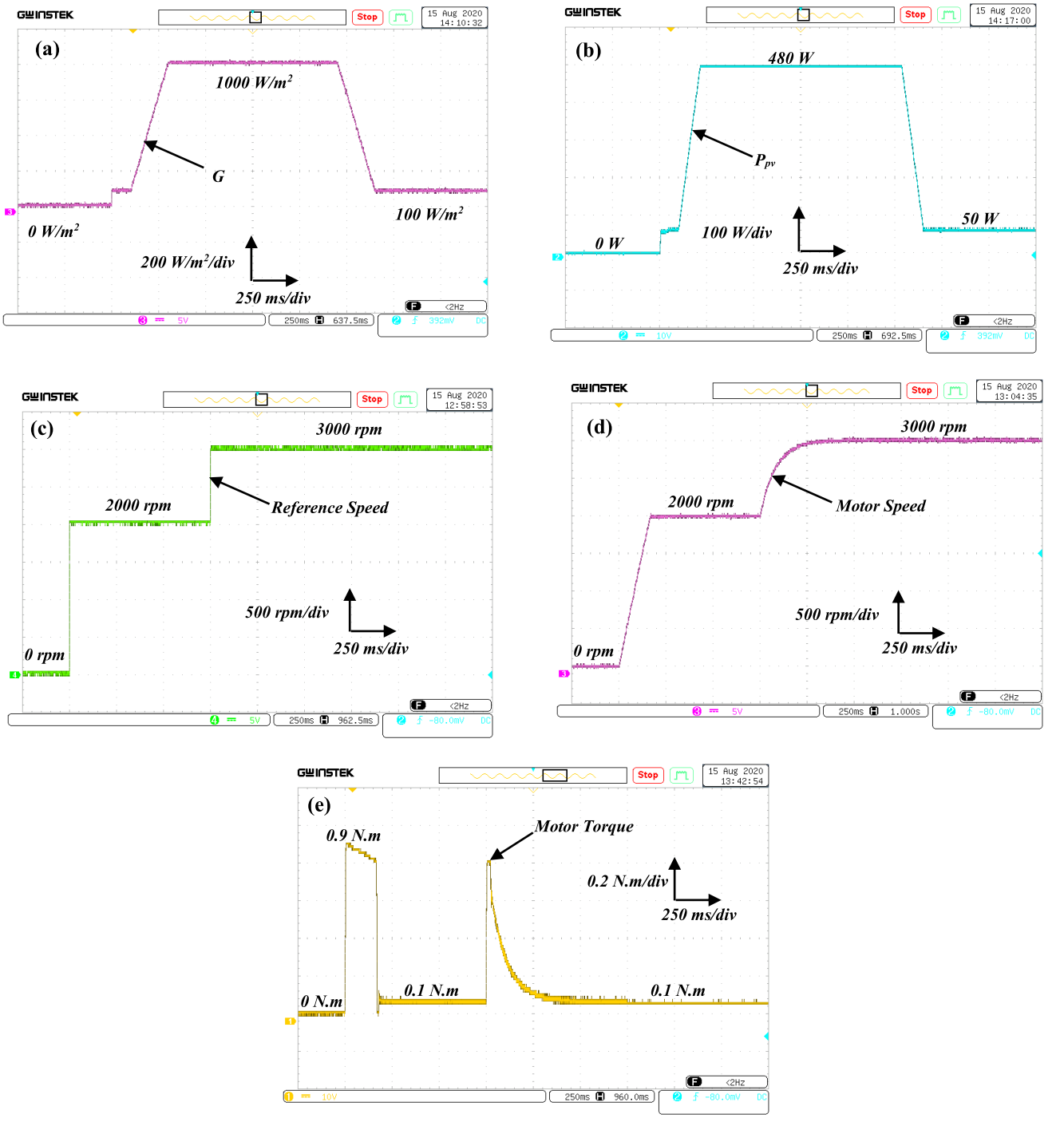

FIGURE 36. Performance of the experimental implementation of FO-Fuzzy-PID regulator-based P&O MPPT and speed control: (a) solar radiation, (b) output power, (c) reference speed, (d) motor speed, (e) motor torque.

programmed into the RAM of the processor. In HIL test, solar PV-WFS it's a Simulink model, not a physical model. Data is transferred between the two parties; dSPACE® ds1104 control panel and the software model via a high-speed serial port. The control system is executed with a 50 μs time-step. Thus, if there are any glitches during the HIL test, it is easy to go back to the code to be rectified. A four-channel, 100 MHz digital mixed-signal oscilloscope was used to record the test results.

Real-time implementation of the proposed PV-WFS was executed under ramp-change in solar irradiance with motor speed and load torque variations. The outcomes are presented

in Fig. 36. The experimental results of the suggested technique show a behavior that is very similar to the simulations, which proves the suitability of the suggested algorithm. The theoretical and the practical results match each other, further illustrating that the dSPACE®1104 board is a powerful and reliable tool for real-time implementation.

VII. CONCLUSION

This document introduces the design and the implementation of a novel control technique based on the FO-Fuzzy-PID regulator with PSO algorithm for WFS to be integrated with a PV power system. This advanced technology is used to enhance the performance of the PV-WFS, particularly in terms of attaining the highest maximum power values, minimizing power ripples, and achieving a fast and robust dynamic response of motor speed. Simulations were carried out in the MATLAB/SIMULINK to demonstrate the efficacy of the considered approach. HIL experiments were conducted based on the dSPACE 1104 DS card to validate the simulation results. The simulation and the experimental results indicate good performances for the proposed control method compared to the traditional control strategies. The key findings of this research are as follows:

1. The proposed PV-WFS combination is a good option for supplying WFS with clean power generation.
2. Applying the PSO algorithm tackled the issue of selecting parameters values of the suggested FO-Fuzzy-PID regulator.
3. The weighted fitness function boosts the FO-Fuzzy-PID regulator to attain best parameters that exhibit the maximum PV power values compared to FLC, FOPID, and PID regulators.
4. The indirect MPPT control algorithm for the reference current generation is efficient for solar PV generator.
5. FO-Fuzzy-PID based P&O MPPT control demonstrates its advantage in attaining maximum energy values with the greatest stability compared to FLC, FOPID and PID based P&O MPPT regulators.
6. The suggested FO-Fuzzy-PID based P&O MPPT control method operates consistently, adaptable, and stable even during situations of top shading. In addition, the developed technique was tested under different weather situations, like the case of intermittent insolation and real climatic data.
7. The proposed FO-Fuzzy-PID regulator provides improved speed regulation of the PMDC motor, reduces rise time, steady-state error, and has a better performance than FLC, FOPID, and PID speed regulators.
8. The studied system is validated experimentally for ramp-change in solar irradiance.
9. A preliminary analysis of the simulation and practical results indicate that they are all in acceptable agreement.

The findings of this document are likely to be beneficial to PV-WFS researchers and developers. Therefore, the proposed PSO based FO-Fuzzy-PID regulator with the improved P&O MPPT method it is an excellent and highly recommended strategy for the PV-WFS, since it may be utilized for any sort of WFS-PV even in cloudy circumstances.

ACKNOWLEDGMENT

The authors thank Taif University Researchers Supporting Project through Taif University, Taif, Saudi Arabia, under Grant TURSP-2020/97 for supporting this work.

The authors express their sincere gratitude to the LEPCI Laboratory of the University of Ferhat Abbas Sétif1, Algeria, for providing particular assistance in the preparation of this manuscript.

REFERENCES

[1] L. Zarour, K. Abed, M. Hacil, and A. Borni, "Control and optimisation of photovoltaic water pumping system using sliding mode," *Bull. Polish Acad. Sci. Tech. Sci.*, vol. 67, no. 3, pp. 1–7, 2019, doi: 10.24425/bpasts.2019.129658.

[2] O. F. Benaouda, B. Babes, M. Bouchakour, S. Kahla, and A. Bendiabdellah, "Arc welding current control using thyristor based three-phase rectifiers applied to gas metal arc welding connected to grid network," *J. Européen Syst. Automatisés*, vol. 54, no. 2, pp. 335–344, Apr. 2021, doi: 10.18280/jesa.540216.

[3] N. Hamouda, B. Babes, S. Kahla, Y. Soufi, J. Petzoldt, and T. Ellinger, "Predictive control of a grid connected PV system incorporating active power filter functionalities," in *Proc. 1st Int. Conf. Sustain. Renew. Energy Syst. Appl. (ICSRESA)*, Tebessa, Algeria, Dec. 2019, pp. 1–6, doi: 10.1109/ICSRESA49121.2019.9182655.

[4] H. Afghoul, F. Krim, A. Beddar, and B. Babes, "Real-time implementation of robust controller for PV emulator supplied shunt active power filter," in *Proc. 6th Int. Renew. Sustain. Energy Conf. (IRSEC)*, Rabat, Morocco, Dec. 2018, pp. 1–6, doi: 10.1109/IRSEC.2018.8703010.

[5] M. Al-Dhaifallah, A. M. Nassef, H. Rezk, and K. S. Nisar, "Optimal parameter design of fractional order control based INC-MPPT for PV system," *Sol. Energy*, vol. 159, pp. 650–664, Jan. 2018, doi: 10.1016/j.solener.2017.11.040.

[6] S.-A. Blaifi, S. Moulahoum, B. Taghezouit, and A. Saim, "An enhanced dynamic modeling of PV module using Levenberg–Marquardt algorithm," *Renew. Energy*, vol. 135, pp. 745–760, May 2019, doi: 10.1016/j.renene.2018.12.054.

[7] R. Khanaki, M. A. M. Radzi, and M. H. Marhaban, "Artificial neural network based maximum power point tracking controller for photovoltaic standalone system," *Int. J. Green Energy*, vol. 13, no. 3, pp. 283–291, Feb. 2016, doi: 10.1080/15435075.2014.910783.

[8] F. Zhang, J. Maddy, G. Premier, and A. Guwy, "Novel current sensing photovoltaic maximum power point tracking based on sliding mode control strategy," *Sol. Energy*, vol. 118, pp. 80–86, Aug. 2015, doi: 10.1016/j.solener.2015.04.039.

[9] M. Kermadi, S. Mekhilef, Z. Salam, J. Ahmed, and E. M. Berkouk, "Assessment of maximum power point trackers performance using direct and indirect control methods," *Int. Trans. Electr. Energy Syst.*, vol. 30, no. 10, pp. 1–18, Oct. 2020, doi: 10.1002/2050-7038.12565.

[10] M. Killi and S. Samanta, "Modified perturb and observe MPPT algorithm for drift avoidance in photovoltaic systems," *IEEE Trans. Ind. Electron.*, vol. 62, no. 9, pp. 5549–5559, Sep. 2015.

[11] B. I. Rani, G. S. Ilango, and C. Nagamani, "Control strategy for power flow management in a PV system supplying DC loads," *IEEE Trans. Ind. Electron.*, vol. 60, no. 8, pp. 3185–3194, Aug. 2013.

[12] B.-R. Peng, K.-C. Ho, and Y.-H. Liu, "A novel and fast MPPT method suitable for both fast changing and partially shaded conditions," *IEEE Trans. Ind. Electron.*, vol. 65, no. 4, pp. 3240–3251, Apr. 2018.

[13] R. Pradhan and B. Subudhi, "Double integral sliding mode MPPT control of a photovoltaic system," *IEEE Trans. Control Syst. Technol.*, vol. 24, no. 1, pp. 285–292, Jan. 2016, doi: 10.1109/TCST.2015.2420674.

[14] E. Bianconi, J. Calvente, R. Giral, E. Mamarelis, G. Petrone, C. A. Ramos-Paja, G. Spagnuolo, and M. Vitelli, "A fast current-based MPPT technique employing sliding mode control," *IEEE Trans. Ind. Electron.*, vol. 60, no. 3, pp. 1168–1178, Mar. 2013.

[15] M. Farhat, O. Barambones, and L. Sbita, "Real-time efficiency boosting for PV systems using MPPT based on sliding mode," *Energy Proc.*, vol. 75, pp. 361–366, Aug. 2015.

[16] A. Kihel, F. Krim, and A. Laib, "MPPT voltage oriented loop based on integral sliding mode control applied to the boost converter," in *Proc. 6th Int. Conf. Syst. Control (ICSC)*, Batna, Algeria, vol. 2, May 2017, pp. 205–209.

[17] M. A. Shamseldin and A. A. El-Samahy, "Speed control of BLDC motor by using PID control and self-tuning fuzzy PID controller," in *Proc. 15th Int. Workshop Res. Educ. Mechatronics (REM)*, Sep. 2014, pp. 1–6.

[18] R. Singhal, S. Padhee, and G. Kaur, "Design of fractional order PID controller for speed control of DC motor," *Int. J. Sci. Res. Publications*, vol. 2, no. 6, pp. 1–8, 2012.

[19] C. A. Monje, Y. Q. Chen, B. M. Vinagre, D. Xue, and V. Feliu, *Fractional-Order Systems and Controls*. London, U.K.: Springer-Verlag, 2010.

[20] C. A. Monje, B. M. Vinagre, V. Feliu, and Y. Chen, "Tuning and auto-tuning of fractional order controllers for industry applications," *Control Eng. Pract.*, vol. 16, no. 7, pp. 798–812, Jul. 2008.

[21] A. Rastogi and P. Tiwari, "Optimal tuning of fractional order PID controller for DC motor speed control using particle swarm optimization," *Int. J. Soft Comput. Eng.*, vol. 3, no. 2, pp. 150–157, 2013.

[22] N. M. H. Norsahperi and K. A. Danapalasingam, "Particle swarm-based and neuro-based FOPID controllers for a twin rotor system with improved tracking performance and energy reduction," *ISA Trans.*, vol. 102, pp. 230–244, Jul. 2020, doi: 10.1016/j.isatra.2020.03.001.

[23] O. Gherouat, A. Hassam, O. Aissa, and B. Babes, "Experimental evaluation of single-phase shunt active power filter based on optimized synergetic control strategy for power quality enhancement," *J. Européen Systèmes Automatisés*, vol. 54, no. 4, pp. 649–659, Aug. 2021, doi: 10.18280/jesa.540415.

[24] M. E. B. Aguilar, D. V. Coury, R. Reginatto, and R. M. Monaro, "Multi-objective PSO applied to PI control of DFIG wind turbine under electrical fault conditions," *Electr. Power Syst. Res.*, vol. 180, Mar. 2020, Art. no. 106081, doi: 10.1016/j.epsr.2019.106081.

[25] B. Babes, A. Boutaghane, N. Hamouda, S. Kahla, H. Kellai, T. Ellinger, and J. Petzoldt, "New optimal control of permanent magnet DC motor for photovoltaic wire feeder systems," in *J. Européen Syst. Automatisés*, vol. 53, no. 6, pp. 811–823, 2020, doi: doi:.10.18280/jesa.530607.

[26] S. Chaouch, M. Hasni, A. Boutaghane, B. Babes, M. Mezaache, S. Slimane, and M. Djenaihi, "DC-motor control using arduino-uno board for wire-feed system," in *Proc. Int. Conf. Electr. Sci. Technol. Maghreb (CISTEM)*, Algiers, Algeria, Oct. 2018, pp. 1–6, doi: 10.1109/CISTEM.2018.8613492.

[27] R. V. Jain, M. V. Aware, and A. S. Junghare, "Tuning of fractional order PID controller using particle swarm optimization technique for DC motor speed control," in *Proc. IEEE 1st Int. Conf. Power Electron., Intell. Control Energy Syst. (ICPEICES)*, Jul. 2016, pp. 1–4.

[28] I. Kurniawan, A. I. Cahyadi, and I. Ardiyanto, "Tuning fractional order proportional integral derivative controller for DC motor control model using cross-entropy method," in *Proc. 3rd Int. Conf. Inf. Technol., Inf. Syst. Electr. Eng. (ICITISEE)*, Yogyakarta, Indonesia, Nov. 2018, pp. 351–356, doi: 10.1109/ICITISEE.2018.8721016.

[29] S. A. Gunawan, Y. C. H. Yuwono, G. N. P. Pratama, A. I. Cahyadi, and B. Winduratna, "Optimal fractional-order PID for DC motor: Comparison study," in *Proc. 4th Int. Conf. Sci. Technol. (ICST)*, Yogyakarta, Indonesia, Aug. 2018, pp. 1–6.

[30] S. Das, I. Pan, and S. Das, "Performance comparison of optimal fractional order hybrid fuzzy PID controllers for handling oscillatory fractional order processes with dead time," *ISA Trans.*, vol. 52, no. 4, pp. 550–566, 2013.

[31] S. Das, I. Pan, S. Das, and A. Gupta, "A novel fractional order fuzzy PID controller and its optimal time domain tuning based on integral performance indices," *Eng. Appl. Artif. Intell.*, vol. 25, no. 2, pp. 430–442, Mar. 2012.

[32] I. Pan and S. Das, "Fractional order fuzzy control of hybrid power system with renewable generation using chaotic PSO," *ISA Trans.*, vol. 62, pp. 19–29, May 2016.

[33] I. S. Jesus and R. S. Barbosa, "Genetic optimization of fuzzy fractional PD+I controllers," *ISA Trans.*, vol. 57, pp. 220–230, Jul. 2015.

[34] T. Mahto and V. Mukherjee, "Fractional order fuzzy PID controller for wind energy-based hybrid power system using quasi-oppositional harmony search algorithm," *IET Gener., Transmiss. Distrib.*, vol. 11, no. 13, pp. 3299–3309, Sep. 2017.

[35] A. Beddar, H. Bouzekri, B. Babes, and H. Afghoul, "Experimental enhancement of fuzzy fractional order PI+I controller of grid connected variable speed wind energy conversion system," *Energy Convers. Manage.*, vol. 123, pp. 569–580, Sep. 2016.

[36] A. Kumar and V. Kumar, "Hybridized ABC-GA optimized fractional order fuzzy pre-compensated FOPID control design for 2-DOF robot manipulator," *AEU-Int. J. Electron. Commun.*, vol. 79, pp. 219–233, Sep. 2017, doi: 10.1016/j.aeue.2017.06.008.

[37] N. Hamouda, B. Babes, C. Hamouda, S. Kahla, T. Ellinger, and J. Petzoldt, "Optimal tuning of fractional order proportional-integral-derivative controller for wire feeder system using ant colony optimization," *J. Européen Syst. Automatisés*, vol. 53, no. 2, pp. 157–166, May 2020, doi: 10.18280/jesa.530201.

[38] R. Sharma, K. P. S. Rana, and V. Kumar, "Performance analysis of fractional order fuzzy PID controllers applied to a robotic manipulator," *Expert Syst. Appl.*, vol. 41, no. 9, pp. 4274–4289, 2014.

[39] Z. Bingul and O. Karahan, "Comparison of PID and FOPID controllers tuned by PSO and ABC algorithms for unstable and integrating systems with time delay," *Optim. Control Appl. Methods*, vol. 39, no. 4, pp. 1431–1450, Jul. 2018, doi: 10.1002/oca.2419.

[40] M.-H. Khooban, M. Gheisarnejad, N. Vafamand, and J. Boudjadar, "Electric vehicle power propulsion system control based on time-varying fractional calculus: Implementation and experimental results," *IEEE Trans. Intell. Veh.*, vol. 4, no. 2, pp. 255–264, Jun. 2019, doi: 10.1109/TIV.2019.2904415.

[41] N. Hamouda, B. Babes, S. Kahla, A. Boutaghane, A. Beddar, and O. Aissa, "ANFIS controller design using PSO algorithm for MPPT of solar PV system powered brushless DC motor based wire feeder unit," in *Proc. Int. Conf. Electr. Eng. (ICEE)*, Istanbul, Turkey, Sep. 2020, pp. 1–6, doi: 10.1109/ICEE49691.2020.9249869.

[42] J.-Y. Cao and B.-G. Cao, "Design of fractional order controllers based on particle swarm optimization," in *Proc. 1st IEEE Conf. Ind. Electron. Appl.*, Singapore, May 2006, pp. 1–6.

[43] M. Karimi-Ghartemani, M. Zamani, N. Sadati, and M. Parniani, "An optimal fractional order controller for an AVR system using particle swarm optimization algorithm," in *Proc. Large Eng. Syst. Conf. Power Eng.*, Montreal, QC, Canada, Oct. 2007, pp. 244–249.

[44] B. Assam, S. Messalti, and A. Harrag, "New improved hybrid MPPT based on backstepping-sliding mode for PV system," *J. Européen Syst. Automatisés*, vol. 52, no. 3, pp. 317–323, Aug. 2019, doi: 10.18280/jesa.520313.

[45] D. Rekioua and E. Matagne, *Optimization of Photovoltaic Power Systems*. London, U.K.: Springer, 2012.

[46] M. Metry, M. B. Shadmand, R. S. Balog, and H. Abu-Rub, "MPPT of photovoltaic systems using sensorless current-based model predictive control," *IEEE Trans. Ind. Appl.*, vol. 53, no. 2, pp. 1157–1167, Mar. 2017.

[47] M. Datta and T. Senjyu, "Fuzzy control of distributed PV inverters/energy storage systems/electric vehicles for frequency regulation in a large power system," *IEEE Trans. Smart Grid*, vol. 4, no. 1, pp. 479–488, Mar. 2013.

[48] M. F. El-Khatib, S. Shaaban, and M. I. A. El-Sebah, "A proposed advanced maximum power point tracking control for a photovoltaic-solar pump system," *Sol. Energy*, vol. 158, pp. 321–331, Dec. 2017, doi: 10.1016/j.solener.2017.09.051.

[49] D. Abbes, A. Martinez, G. Champenois, and B. Robyns, "Real time supervision for a hybrid renewable power system emulator," *Simul. Model. Pract. Theory*, vol. 42, pp. 53–72, Mar. 2014, doi: 10.1016/j.simpat.2013.12.003.

[50] B. Babes, A. Boutaghane, N. Hamouda, M. Mezaache, and S. Kahla, "A robust adaptive fuzzy fast terminal synergetic voltage control scheme for DC/DC buck converter," in *Proc. Int. Conf. Adv. Elect. Eng. (ICAEE)*, Algiers, Algeria, 2019, pp. 1–5, doi: 10.1109/ICAEE47123.2019.9014717.

[51] B. Babes, A. Boutaghane, N. Hamouda, and M. Mezaache, "Design of a robust voltage controller for a DC–DC buck converter using fractional-order terminal sliding mode control strategy," in *Proc. Int. Conf. Adv. Electr. Eng. (ICAEE)*, Algiers, Algeria, Nov. 2019, pp. 1–6, doi: 10.1109/ICAEE47123.2019.9014788.

[52] N. Hamouda, B. Babes, and A. Boutaghane, "Design and analysis of robust non-linear synergetic controller for a PMDC motor driven wire-feeder system (WFS)," in *Proc. 4th Int. Conf. Electr. Eng. Control Appl. (ICEECA)*, in Lecture Notes in Electrical Engineering, vol. 682, S. Bououden, M. Chadli, S. Ziani, and I. Zelinka, Eds. Singapore: Springer, 2021, doi: 10.1007/978-981-15-6403-1_26.

[53] H. Afghoul, F. Krim, B. Babes, A. Beddar, and A. Kihel, "Design and real time implementation of sliding mode supervised fractional controller for wind energy conversion system under sever working conditions," *Energy Convers. Manage.*, vol. 167, pp. 91–101, Jul. 2018.
[54] S. Kahla, M. Bechouat, T. Amieur, M. Sedraoui, B. Babes, and N. Hamouda, "Maximum power extraction framework using robust fractional-order feedback linearization control and GM-CPSO for PMSG-based WECS," *Wind Eng.*, vol. 45, no. 4, pp. 1040–1054, Aug. 2021, doi: 10.1177/0309524X20948263.
[55] N. Hamouda, B. Babes, A. Boutaghane, S. Kahla, and M. Mezaache, "Optimal tuning of $PI^{\lambda}D^{\mu}$ controller for PMDC motor speed control using ant colony optimization algorithm for enhancing robustness of WFSs," in *Proc. 1st Int. Conf. Commun., Control Syst. Signal Process. (CCSSP)*, El Oued, Algeria, May 2020, pp. 364–369, doi: 10.1109/CCSSP49278.2020.9151609.
[56] N. Hamouda, B. Babes, S. Kahla, C. Hamouda, and A. Boutaghane, "Particle swarm optimization of fuzzy fractional PD+I controller of a PMDC motor for reliable operation of wire-feeder units of GMAW welding machine," *Przegląd Elektrotechniczny*, vol. 96, pp. 40–46, Nov. 2020, doi: 10.15199/48.2020.12.07.
[57] R. Eberhart and J. Kennedy, "A new optimizer using particle swarm theory," in *Proc. 6th Int. Symp. Micro Mach. Hum. Sci.*, 1995, pp. 39–43, doi: 10.1109/MHS.1995.494215.
[58] A. Krama, L. Zellouma, A. Benaissa, B. Rabhi, M. Bouzidi, and M. F. Benkhoris, "Design and experimental investigation of predictive direct power control of three-phase shunt active filter with space vector modulation using anti-windup PI controller optimized by PSO," *Arabian J. Sci. Eng.*, vol. 44, no. 8, pp. 6741–6755, Aug. 2019.
[59] M. Qais, H. M. Hasanien, and S. Alghuwainem, "Salp swarm algorithm-based TS-FLCs for MPPT and fault ride-through capability enhancement of wind generators," *ISA Trans.*, vol. 101, pp. 211–224, Jun. 2020, doi: 10.1016/j.isatra.2020.01.018.
[60] D. Sera, L. Mathe, T. Kerekes, S. V. Spataru, and R. Teodorescu, "On the perturb-and-observe and incremental conductance MPPT methods for PV systems," *IEEE J. Photovolt.*, vol. 3, no. 3, pp. 1070–1078, Jul. 2013.
[61] A. S. Benyoucef, A. Chouder, K. Karaa, S. Silvestre, and O. A. Sahed, "Artificial bee colony based algorithm for maximum power point tracking (MPPT) for PV systems operating under partial shaded conditions," *Appl. Soft Comput.*, vol. 32, nos. 38–48, Jul. 2015.

BADREDDINE BABES received the B.Eng. and M.Sc. degrees in electrical engineering from the University of Setif-1, Algeria, in 2004 and 2010, respectively, and the Ph.D. degree in electrical engineering from the University of Setif-1, in 2018, with specialization in electric drive applications and controls. He joined the Research Center in Industrial Technologies (CRTI), Algiers, Algeria, in 2017, as an Assistant Researcher. He is currently working as a Senior Researcher "A" at CRTI. His research interests include power electronic converters, power factor correction, and solar energy.

FAHAD ALBALAWI received the master's degree in electrical engineering from George Washington University, in 2013, and the Ph.D. degree in electrical engineering from UCLA, in 2017. He is currently an Associate Professor at the Electrical Engineering Department, Taif University. His research interests include the fields of nonlinear control theory, mode predictive control, and learning-based control algorithms.

NOUREDDINE HAMOUDA received the Engineering degree in electrical engineering from the University of Jijel, Algeria, in 2006, the Magister degree from the Department of Electrical Engineering, Ferhat Abbas Setif University 1, Algeria, in 2010, the Ph.D. degree in electrical engineering from the University of Mentouri Brothers Constantine, Algeria, in 2018, and the Habilitation degree from 8 Mai 1945 Guelma University, Algeria, in 2021. From 2010 to 2012, he was with Razal-CMC Company French–Italy as an Engineer in electrical engineering. Since 2013, he has been with the Research Center in Industrial Technologies (CRTI), Algiers, Algeria. He has authored or coauthored 18 papers in power electronics, active power filter, renewable energy systems, welding systems control, and optimization techniques.

SAMI KAHLA received the B.Sc. and Magister degrees in automatic from Tebessa University, Algeria, in 2009 and 2013, respectively, and the Ph.D. degree in electrical engineering from the University of Guelma, Algeria, in 2018. He is currently a Senior Researcher at the Research Center in Industrial Technologies (CRTI), Algiers, Algeria. His research interests include power energy conversion systems, fuzzy logic control (FLC), metaheuristic optimization algorithms, and power electronics.

SHERIF S. M. GHONEIM (Senior Member, IEEE) received the B.Sc. and M.Sc. degrees from the Faculty of Engineering at Shoubra, Zagazig University, Egypt, in 1994 and 2000, respectively, and the Ph.D. degree in electrical power and machines from the Faculty of Engineering, Cairo University, in 2008. Since 1996, he has been teaching with the Faculty of Industrial Education, Suez Canal University, Egypt. From 2005 to 2007, he was a Guest Researcher with the Institute of Energy Transport and Storage (ETS), University of Duisburg-Essen, Germany. He joined the Electrical Engineering Department, Faculty of Engineering, Taif University, as an Associate Professor. His research interests include grounding systems, breakdown in SF6 gas, dissolved gas analysis, and AI technique applications.